Electronic Supplementary Information

Towards water-tolerant *ansa*-aminoboranes for parahydrogen-induced polarization and beyond

Karolina Konsewicz,[a] Timo Repo[b] and Vladimir V. Zhivonitko*[a]

[a.] NMR Research Unit, Faculty of Science, University of Oulu, P.O. Box 3000, Oulu, 90014, Finland. E-mail: vladimir.zhivonitko@oulu.fi.

[b.] Department of Chemistry, University of Helsinki, A. I. Virtasen Aukio 1, 00014 Helsinki, Finland.

-CONTENTS-

-LIST OF FIGURES-

-LIST OF TABLES-

1 Materials and experimental methods

1.1 Substance names

MesCAT: 1-(2-(dimesitylboraneyl)phenyl)-2,2,6,6-tetramethylpiperidine
MesCAT-H_2: dimesityl(2-(2,2,6,6-tetramethylpiperidin-1-ium-1-yl)phenyl)hydroborate
MesCAT-H_2O: hydroxydimesityl(2-(2,2,6,6-tetramethylpiperidin-1-ium-1-yl)phenyl)borate
PhCAT: 1-(2-(diphenylboraneyl)phenyl)-2,2,6,6-tetramethylpiperidine
PhCAT-H_2: diphenyl(2-(2,2,6,6-tetramethylpiperidin-1-ium-1-yl)phenyl)hydroborate
PhCAT-H_2O: hydroxydiphenyl(2-(2,2,6,6-tetramethylpiperidin-1-ium-1-yl)phenyl)borate
para-H_2: parahydrogen

1.2 Abbreviations

NS: number of accumulations, NS parameter in NMR pulse sequences.

1.3 General information

NMR experiments with parahydrogen were performed on a 400 MHz Bruker AV 400 NMR spectrometer equipped with a broad-band 5 mm RF probe. The kinetic (k'_{as}, k'_{dis}) parameter measurements were performed on a 600 MHz Spectrometer Bruker AV 600 NMR equipped with a broad-band 5 mm RF probe. The standard temperature control units of the NMR spectrometers were used for cooling and heating the samples. The temperature control units were calibrated using a standard NMR thermometer methanol sample.

High-purity H_2 gas was used for producing parahydrogen-enriched H_2, referred to in the main text as simply parahydrogen. The enrichment was performed with a Bruker parahydrogen generator, which produced H_2 gas with 92 % of parahydrogen.

1.4 Sample preparation

The initial ^{15}N-labelled *ansa*-aminoboranes (AABs), **MesCAT-**^{15}N and **PhCAT-**^{15}N, referred to in the text without the "^{15}N" ending, were synthesized as per the original method; these compounds are known.[S1] Their water adducts (**MesCAT-H_2O** and **PhCAT-H_2O**) were prepared by making a slurry of the AABs in water-containing acetonitrile-d3 and separating the resulting residues from the solution followed by a gentle drying on air. After weighing the necessary amounts of the AAB-H_2O, the solid material was dissolved in water-containing acetonitrile-d3 or toluene-d8 for NMR experiments. This procedure provided ca. 1 mM solutions of **MesCAT-H_2O** and **PhCAT-H_2O**. The **MesCAT-H_2O** ÷ H_2O ratios were ca. 1 ÷ (100±10) and 1 ÷ (7±1) in acetonitrile-d3 and toluene-d8, respectively. The **PhCAT-H_2O** ÷ H_2O ratios were ca. 1 ÷ (30±10) and 1 ÷ (7±1) in acetonitrile-d3 and toluene-d8, respectively.

The water-containing solvents were prepared by adding calculated amounts of high-purity deionized water to 1 mL and 5 mL of dry (molecular sieves 0.3 nm) acetonitrile-d3 and toluene-d8,

respectively, by using a VWR micropipette (0.5-10 uL range). The mass change of the solvent aliquots after the addition of water was validated using an analytical balance to control the performance of the micropipette. The volume change was neglected as the amount of the added water was small. Additionally, the AAB-H_2O ÷ H_2O ratios were confirmed by integrating the corresponding signals of NH groups of AAB-H_2O and H_2O as illustrated in Figure S1 and discussed in the next section. The solubility of water in toluene-d8 was significantly limited, and, therefore, the AAB-H_2O ÷ H_2O ratios were significantly bigger than those for acetonitrile-d3.

1.4.1 Comparison of MesCAT-H_2O and H_2O signal intensities

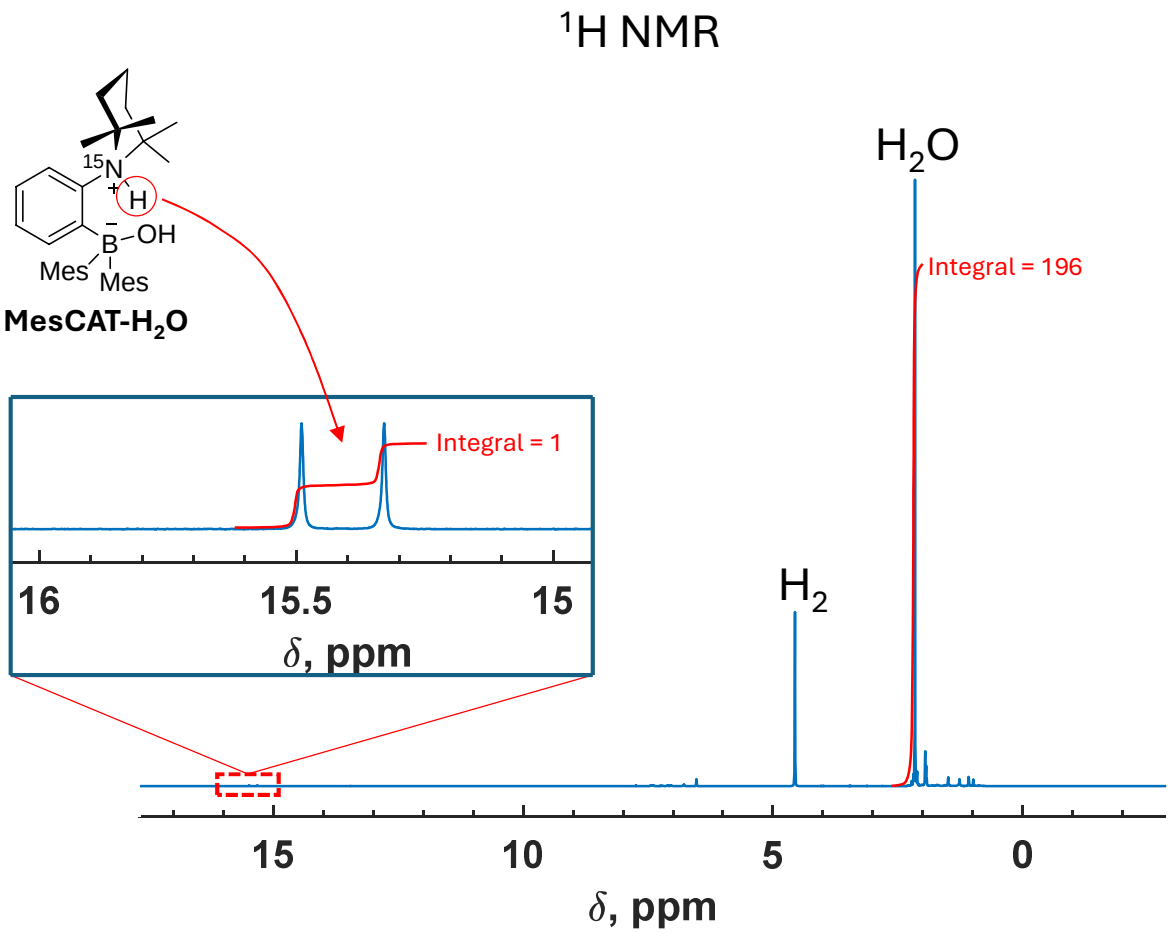

Figure S1. The thermal ^{1}H NMR spectrum measured after parahydrogen experiments with a 1 mM solution of **MesCAT-H_2O** in 0.6 ml of water-containing acetonitrile-d3 (room temperature). Cumulative integral curves and the integral values for the NH signal of **MesCAT-H_2O** and H_2O signal are shown with the red traces.

The spectrum in the figure above illustrated that ^{1}H NMR confirms that the **MesCAT-H_2O** ÷ H_2O ratio was ca. 1 ÷ 100 after the sample preparation. This is visible from the integral values of the NH signal of **MesCAT-H_2O** and H_2O signal. Note that as the H_2O signal corresponds to two protons, its integral must be divided by the factor of two to get the right **MesCAT-H_2O** ÷ H_2O ratio.

1.5 PHIP NMR

1.5.1 Parahydrogen experiments

The experiments were set by charging 5 mm gas-tight NMR sample tubes with the 0.6 mL of the 1 mM solutions of the AAB-H_2O water adducts (**MesCAT-H_2O** or **PhCAT-H_2O**) in water-containing (see above) acetonitrile-d3 or toluene-d8 and adding 6 bars of parahydrogen. After a rigorous shaking, the tubes were inserted onto the NMR magnet for the measurements. $\pi/4$- and $\pi/2$-pulses were used to acquire ^{1}H and ^{11}B NMR spectra, respectively. According to the PASADENA theory in the weak coupling case, the $\pi/4$-pulses maximize the observed hyperpolarized antiphase ^{1}H NMR signals.[S2] The hyperpolarization was observed for a long time (at least 10 min stably) inside the magnet without a need for parahydrogen refreshment. PASADENA-type antiphase signals were detected in the spectra in all cases. This approach allowed for variable temperature measurements since the temperature stabilization was achieved in about 3 min after the sample insertion into the magnet.

We note that due to the variable temperature experiments were used in this study, the concentration of the dissolved para-H_2 can slightly vary with the temperature,[S3,4] leading to a slight increase in the concentration in acetonitrile by a factor of 1.2 if the temperature changes from 297 to 328 K.[S3] We do not expect that this rather slight change in the solubility should change any conclusions regarding the reaction mechanisms in this study.

1.5.2 Estimation of ^{1}H NMR signal enhancements

The ^{15}N-H group proton was chosen to estimate the signal enhancements since the ^{11}B-H group proton antiphase doublets have significantly lower amplitudes due to the strong ^{1}H line broadening induced by the neighboring spin-3/2 quadrupolar ^{11}B, leading to a strong mutual cancellation of the antiphase multiplet components for the ^{11}B-H group signal (four antiphase doublets, see ^{1}H NMR spectra in Section 3.1).

The following procedure was used to estimate average signal enhancements for the NH-group proton of MesCAT-H_2 (Figure 2 in the main text). First, we took into account that this signal corresponds to the AMX type multiplet due to two *J*-couplings: (1) ^{HH}J coupling (ca. 4 Hz) to the BH proton and (2) ^{NH}J (ca. 72 Hz) to the ^{15}N nucleus. Figure S2 shows model thermal (top trace) and hyperpolarized PASADENA-type (bottom trace) signals with artificially narrowed linewidths (1 Hz) to make all multiplet components (1 to 4) completely resolved. In the experiments, these components are not resolved very well due to the significant line broadening of ca. 4 Hz. In addition, the hyperpolarized signals may show deviations from the ideal antiphase patterns, for instance, due to the

influence of cross-correlated relaxation,[S1] not ideal pulse calibrations, or B_1 inhomogeneities. However, it is still possible to estimate the average signal enhancement using the following procedure, and Figure S2 greatly helps to describe our approach.

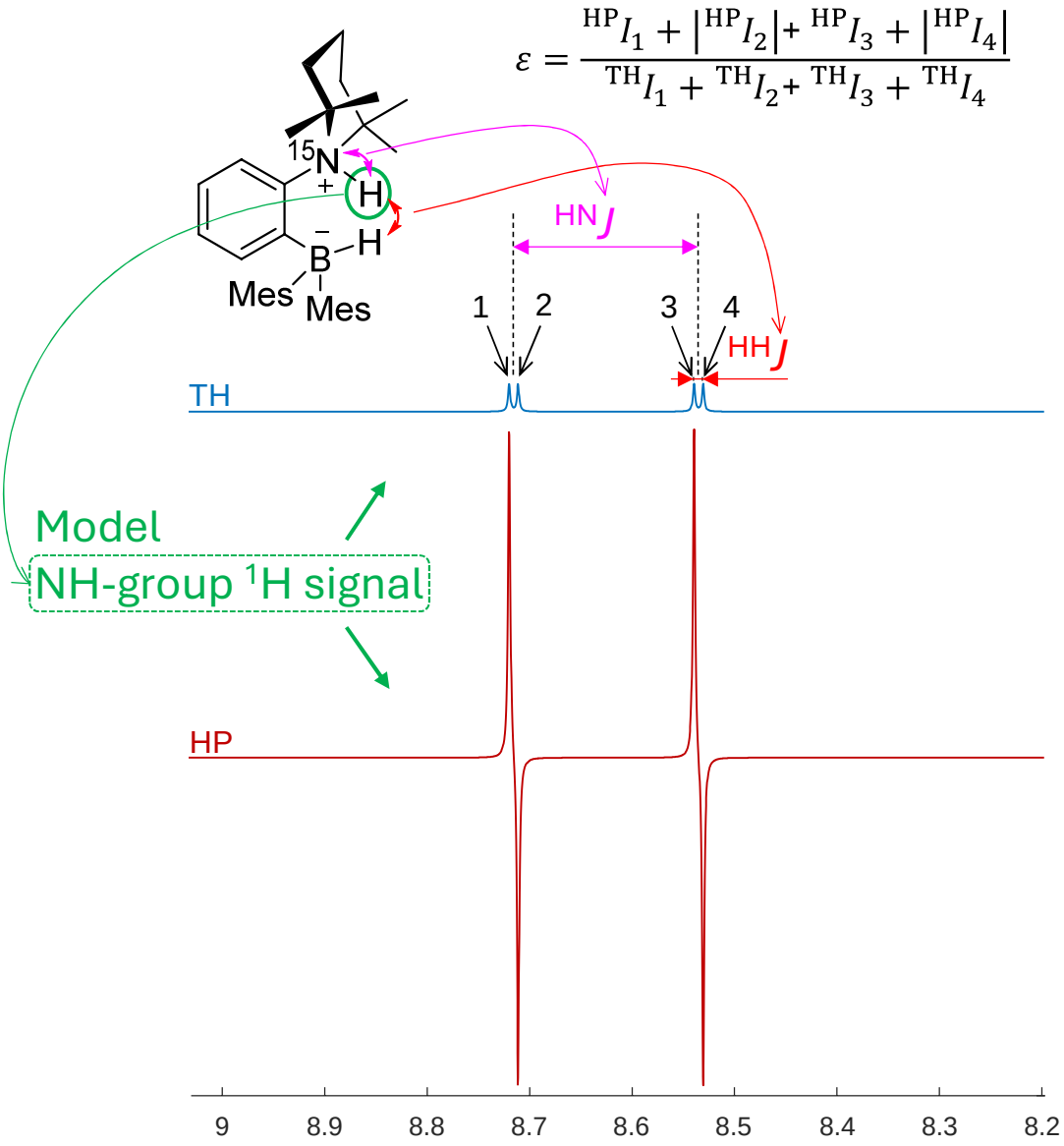

Figure S2. The modeled ^{1}H NMR multiplet lineshapes that correspond to the NH-group proton of **MesCAT-H$_2$** for thermal (top) and hyperpolarized (PASADENA experiment) molecules. In the model, 1 Hz linewidths were used to show clearly all four multiplet components of AMX-spin system pattern resolved, where ^{HN}J is ca. 72 Hz and ^{HH}J is ca. 4 Hz. This schematic presents the idea of the equation on the top that was used to calculate estimates of the observed ^{1}H signal enhancements based on integral amplitudes of the multiplet components 1-4 for thermal ($^{TH}I_i$) and hyperpolarized ($^{HP}I_i$) spectra.

As there are four components that in the thermal spectrum should have approximately the same integral amplitudes, the average signal enhancement factors can be estimated using the following formula:

$$\varepsilon = \frac{^{HP}I_1 + \left|^{HP}I_2\right| + {}^{HP}I_3 + \left|^{HP}I_4\right|}{^{TH}I_1 + {}^{TH}I_2 + {}^{TH}I_3 + {}^{TH}I_4}, \qquad \text{(eq S1)}$$

where $^{HP}I_i$ (i = 1,2,3,4) are integral amplitudes of the multiplet components in the hyperpolarized spectra, whereas $^{TH}I_i$ are their corresponding thermal counterparts. Note that the absolute values of $^{HP}I_2$ and $^{HP}I_4$ are used in the formula to take into account that these multiplet components have negative signs (Figure S2, bottom trace).

In order to use this equation, it is enough to perform numerical integrations of the corresponding NMR signals in the NMR spectra and normalize the obtained integrals $^{HP}I_i{}^0$ and $^{TH}I_i{}^0$ with respect to the number of scan accumulations used in the hyperpolarized and the thermal spectra to obtain the $^{HP}I_i$ and $^{TH}I_i$ values, respectively. This requirement reads as follows:

$$^{HP}I_i = \frac{^{HP}I_i{}^0}{^{HP}\mathrm{NS}} \qquad \text{(eq S2)}$$

and

$$^{TH}I_i = \frac{^{TH}I_i{}^0}{^{TH}\mathrm{NS}}, \qquad \text{(eq S3)},$$

where ^{HP}NS (typically 1 or 8 depending on the temperature) and THNS (3072) are the number of scan accumulations for the hyperpolarized and thermal spectra, respectively.

We note that in the case of the hyperpolarized signals, it was relatively straightforward to perform piecewise numerical integration of all four components ($^{HP}I_i{}^0$) separately because the hyperpolarized components clearly differ by the signs of their phases (absorption, emission, absorption, emission). At the same time, we note that due to the substantial mutual cancellation of these components, as they have opposite phase signs, the integrals $^{HP}I_i = {}^{HP}I_i{}^0 / {}^{HP}\mathrm{NS}$ substitute into the numerator of eq S1 gives the underestimated values of the "real" integrals, and therefore the obtained signal enhancement factors are also underestimated. They should be bigger.

In the case of the integrals of the thermal signals ($^{TH}I_i$), all four multiplet components have the same phase, and it is convenient to obtain the whole sum in the denominator in eq S1 ($^{TH}I_1 + {}^{TH}I_2 + {}^{TH}I_3 + {}^{TH}I_4$) by the integration of the whole NH-group multiplet in the thermal spectra giving $^{TH}I_1^0 + {}^{TH}I_2^0 + {}^{TH}I_3^0 + {}^{TH}I_4^0$ and division of the result by number scan accumulations (THNS) without the need to integrate four separate ranges.

However, the thermal signals of **MesCAT-H₂** had very low intensity, which introduced a significant error in the determination of estimates of the signal enhancement factors using eq S1. At

the same time, we estimated this error based on the noise level present in the numerical integral sum ${}^{\mathrm{TH}}I_{\Sigma}^{0} = {}^{\mathrm{TH}}I_{1}^{0} + {}^{\mathrm{TH}}I_{2}^{0} + {}^{\mathrm{TH}}I_{3}^{0} + {}^{\mathrm{TH}}I_{4}^{0}$. For example, Figure S3 shows a representative thermal signal of **MesCAT-H₂** obtained in the thermal spectrum at 328 K measured after the corresponding PHIP experiment. The noise level is high, but after the whole range integration illustrated by the red trace, we estimated that the noise of the numerical integration ($\Delta^{\mathrm{TH}}I_{\Sigma}^{0}$) is on the 20% with respect to the whole integral (${}^{\mathrm{TH}}I_{\Sigma}^{0}$). This number was used to estimate the error of the obtained experimental enhancement factors shown in Table 1 of the main manuscript. As was mentioned above, we believe that these estimates are actually lower limits because the mutual cancellation effect in the antiphase double components reduces the hyperpolarized signal integrals (${}^{\mathrm{HP}}I_{i}{}^{0}$). Further increase in accuracy is possible by modelling the cancellation effect and measuring thermal spectra with better signal-to-noise, but the obtained values and accuracy were good enough to draw reliable conclusions for this communication about water tolerance of the **MesCAT** compound.

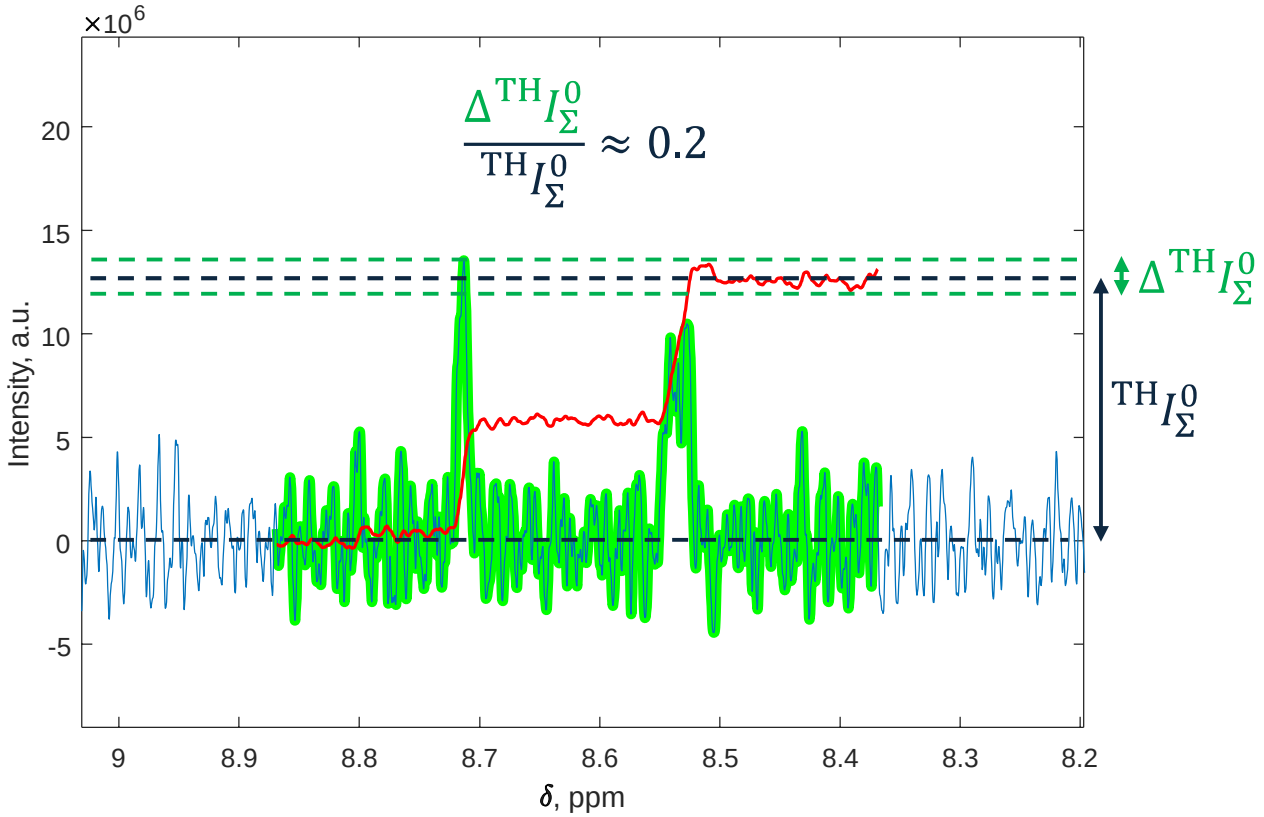

Figure S3. A representative thermal ^{1}H NMR spectrum measured after parahydrogen experiments with a 1 mM solution of **MesCAT-H₂O** in 0.6 ml of water-containing acetonitrile-d3 at 328 K. The cumulative integral curve for the NH-group signal multiplet of **MesCAT-H₂** is shown with the red trace. The beginning and the end of this curve illustrate the level of noise for the numerical integration procedure, which was estimated as 0.2 (20%) based on the ratio of the noise amplitude ($\Delta^{\mathrm{TH}}I_{\Sigma}^{0}$) to the numerical integral of all four multiplet components of NH-group (${}^{\mathrm{TH}}I_{\Sigma}^{0}$).

1.5.3 ^{11}B NMR spectra from parahydrogen experiments with MesCAT-H_2O in acetonitrile-d3

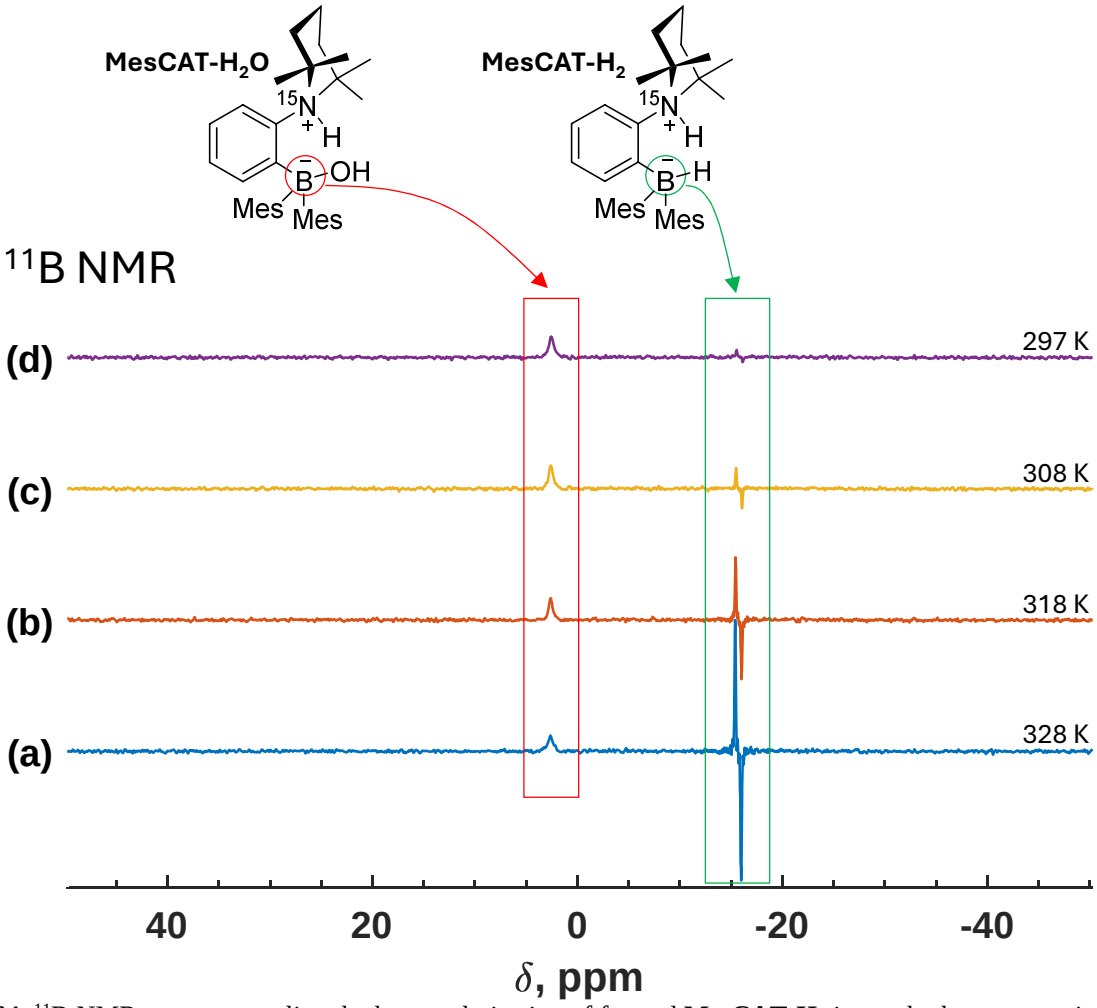

Figure S4. ^{11}B NMR spectra revealing the hyperpolarization of formed **MesCAT-H_2** in parahydrogen experiments with a 1 mM solution of **MesCAT-H_2O** in 0.6 ml of water-containing acetonitrile-d3 at various temperatures (297-328 K).

1.5.4 NMR spectra from parahydrogen experiments with MesCAT-H_2O in toluene-d8

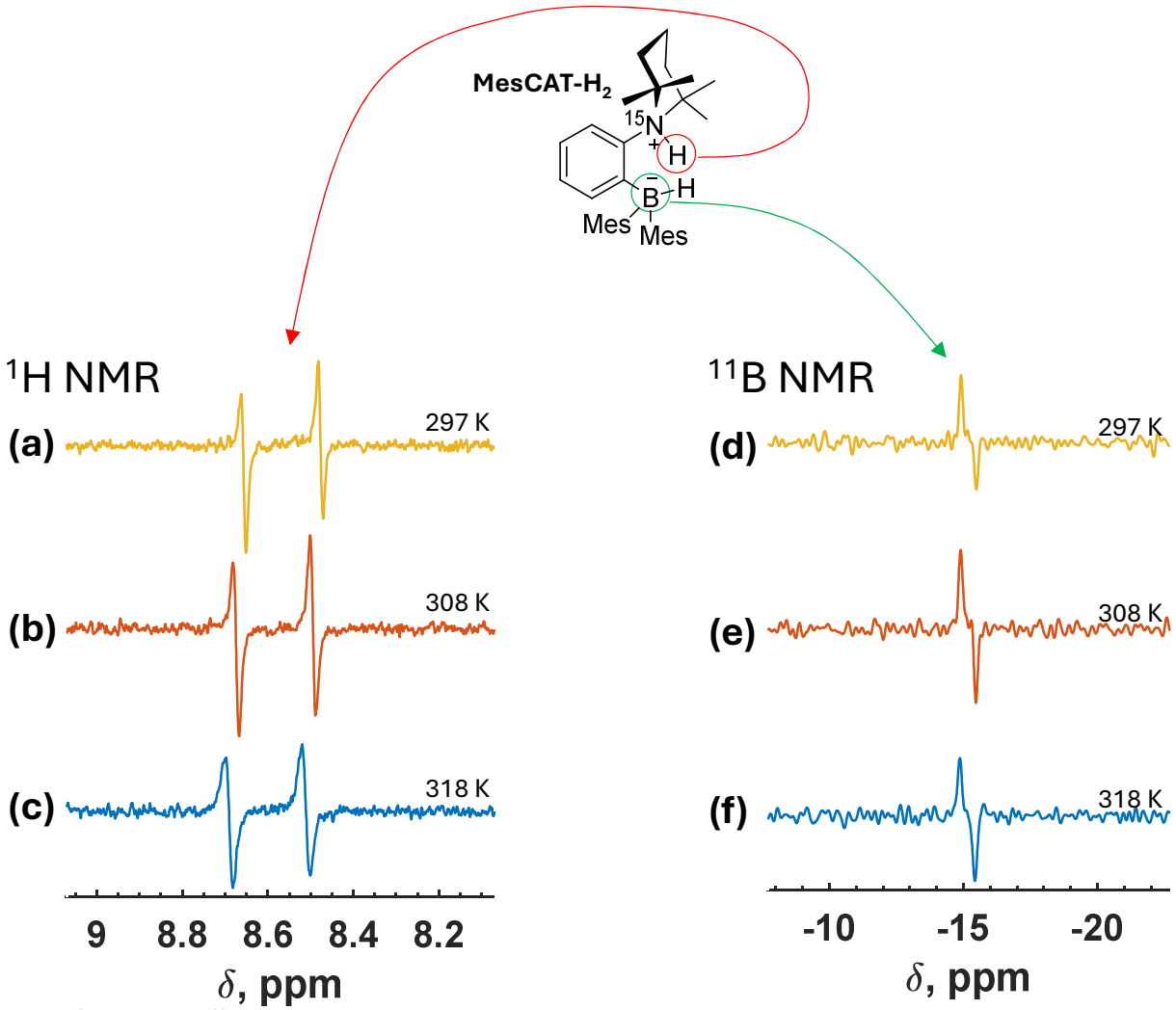

Figure S5. ^{1}H (a-c) and ^{11}B (d-f) NMR spectra revealing the hyperpolarization of formed **MesCAT-H_2** in parahydrogen experiments with a 1 mM solution of **MesCAT-H_2O** in 0.6 ml of water-containing toluene-d8 at various temperatures (297-328 K).

The signal enhancements for **MesCAT-H_2O** experiments in toluene-d8 (see the main text) were determined by the comparison to the noise level in the following experiments with thermal polarization after acquiring 3072 scan averages. In contrast to the acetonitrile experiments, no thermal signal for **MesCAT-H_2** was detected in toluene-d8. This solvent effect is in agreement with previously reported data highlighting that the **MesCAT-H_2** concentration in toluene should be significantly smaller than in acetonitrile under otherwise similar conditions.[S5]

1.6 Kinetic measurements of AAB-H_2O dissociation

The kinetic rates for the dissociation of AAB-H_2O were measured using 1D EXSY NMR (*selnogpzs.2* Bruker experiment) by selective excitation of the NH group proton of **MesCAT-H_2O**

and variation of the exchange time. The following mixing times were used in the experiments (s): 0.02, 0.04, 0.10, 0.15, 0.20, 0.30, 0.4, 0.6, 0.8, 1.00, 1.20, 1.60, 2.40, 3.20, 4.80, 6.40. The number of scans was 16, and the recycling delay was 5 s. The measured EXSY curves, as well as the curves obtained from the data fitting procedures, are shown in the figures of Section 1.6.2 for various temperatures and solvents (acetonitrile-d3 and toluene-d8). For the details of the fitting procedure see Section 1.6.1. The obtained kinetic parameters are presented in the main text and in the Section 1.6.3 in more detail.

1.6.1 Details of the 1D EXSY NMR data fitting

A two-site exchange model[S6] was used to build the model of the magnetization transfer between the NH proton of **MesCAT-H_2O** and free H_2O according to the hydration chemical equilibrium shown in Fig. 1A (top) of the main manuscript. Generally, the following fitting parameters were varied: $k_{as}^{eff} = k'_{as}[\mathrm{MesCAT}]$ – effective H_2O association rate constant that includes equilibrium concentration of **MesCAT** at a given temperature, k'_{dis} – **MesCAT-H_2O** dissociation rate constant, r'_1 – longitudinal relaxation rate of the NH proton of **MesCAT-H_2O**, r_1 – longitudinal relaxation rate of H_2O protons, *A* – scaling coefficient. The fitting model function was evaluated numerically in MATLAB, using the following matrix equation:

$$S_{EXSY}(t) = \begin{pmatrix} S_{EXSY}^{NH}(t) \\ S_{EXSY}^{H_2O}(t) \end{pmatrix} = A \cdot \exp\left[\begin{pmatrix} -r'_1 - k'_{dis} & k_{as}^{eff} \\ k'_{dis} & -r_1 - k_{as}^{eff} \end{pmatrix} t\right] \cdot \begin{pmatrix} 1 \\ 0 \end{pmatrix}, \qquad \text{(eq S4)}$$

predicting points of the kinetic curves for the signal vector $S_{EXSY}(t)$. To improve the quality of the fitting procedure reducing the number of fitted parameters, the k_{as}^{eff} parameter was set to $k_{as}^{eff} = k'_{dis} 2S^{NH}/S^{H_2O}$ based on the fact that under equilibrium conditions the $2S^{NH}/S^{H_2O}$ ratio reflects the [MesCAT-H_2]/[H_2O] ratio, which is equal to k_{as}^{eff}/k'_{dis}.

The fitting procedure was performed in MATLAB using *nlinfit* function. The confidence intervals were estimated using *nlparci* function. Authors are happy to discuss the details or provide advice on using this approach, please contact us.

The next subsections show the results of the fitting procedure along with the experimental points for the NH group signal of **MesCAT-H_2O** and H_2O in the 1D EXSY experiments.

1.6.2 Kinetics plots used to determine k'_{dis} and k'_{as} reaction rates

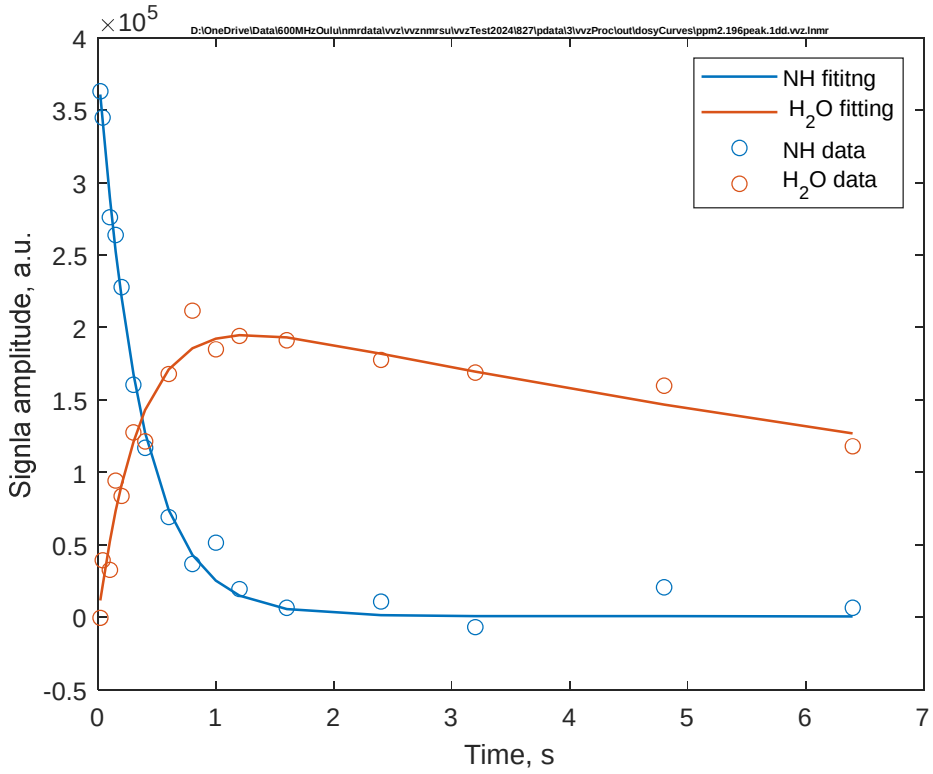

Figure S6. Kinetic curves obtained from 1D EXSY ^{1}H NMR for **MesCAT-H$_2$O** at 294 K in acetonitrile-d3. The integral data points for NH and H$_2$O signals are shown with circles (see legend). The corresponding least-squares fits are shown with the solid lines.

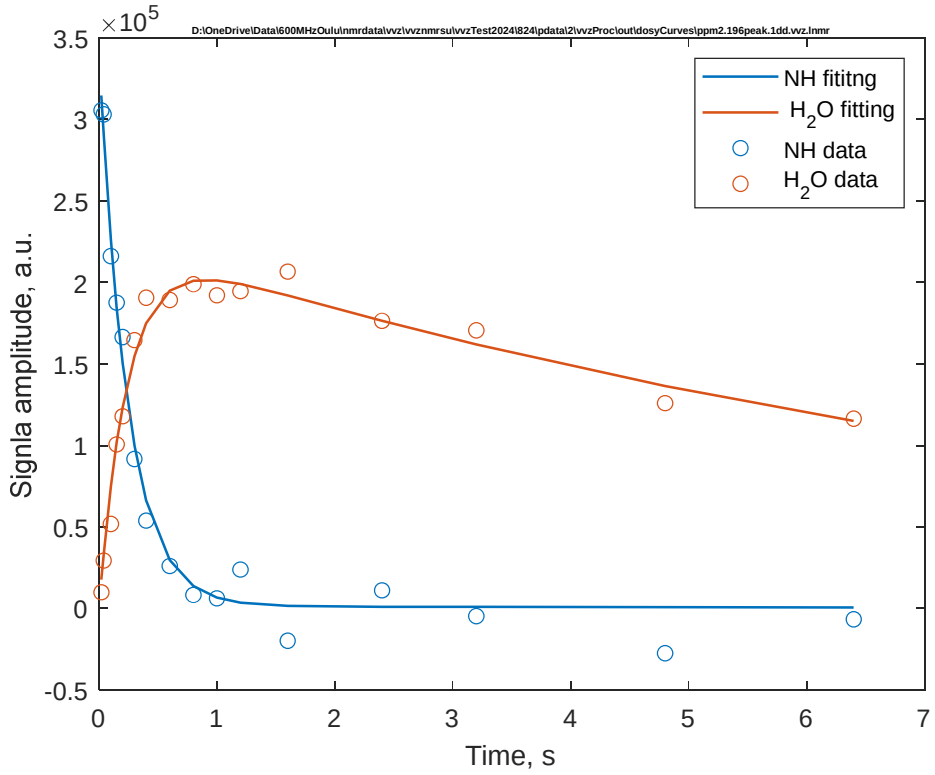

Figure S7. Kinetic curves obtained from 1D EXSY ^{1}H NMR for **MesCAT-H$_2$O** at 298 K in acetonitrile-d3. The integral data points for NH and H_2O signals are shown with circles (see legend). The corresponding least-squares fits are shown with the solid lines.

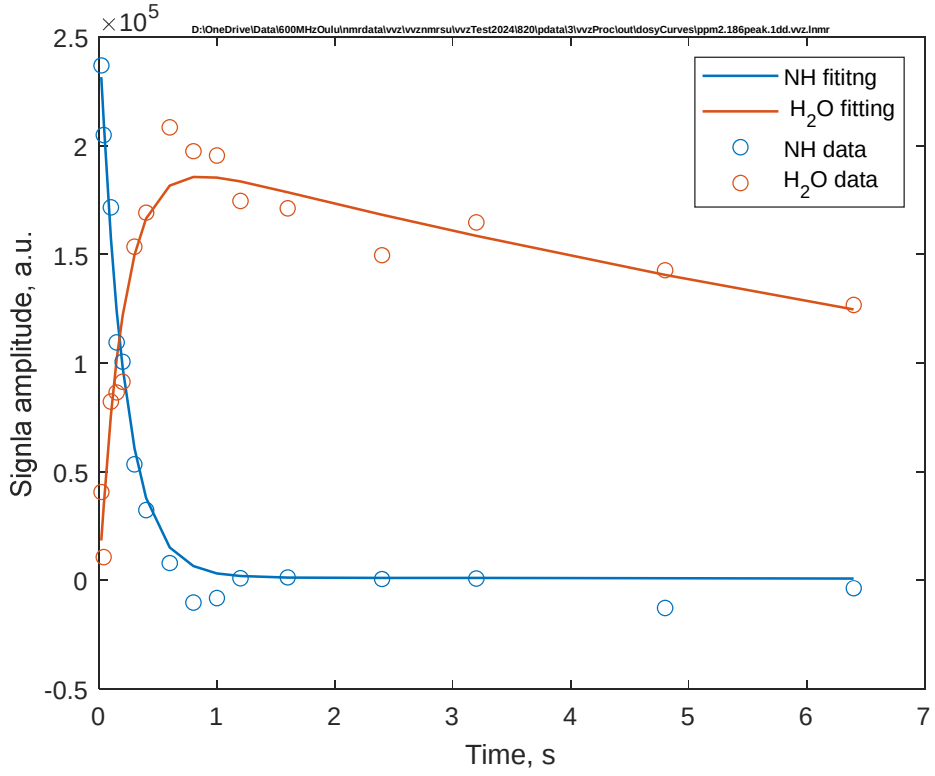

Figure S8. Kinetic curves obtained from 1D EXSY ^{1}H NMR for **MesCAT-H$_2$O** at 302 K in acetonitrile-d3. The integral data points for NH and H_2O signals are shown with circles (see legend). The corresponding least-squares fits are shown with the solid lines.

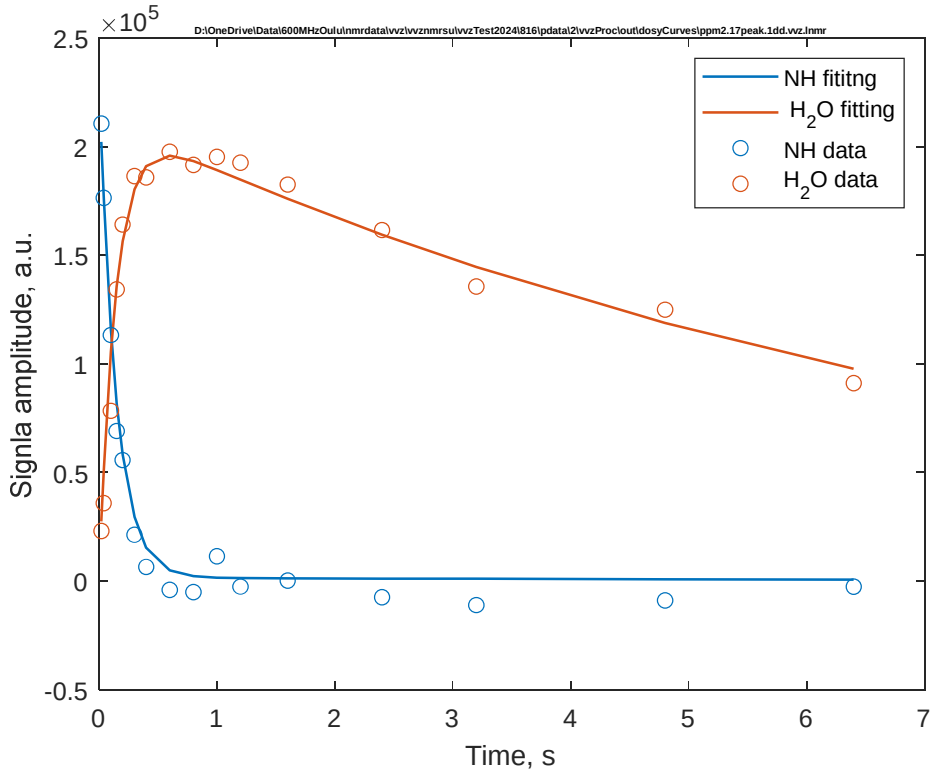

Figure S9. Kinetic curves obtained from 1D EXSY ^{1}H NMR for **MesCAT-H$_2$O** at 306 K in acetonitrile-d3. The integral data points for NH and H_2O signals are shown with circles (see legend). The corresponding least-squares fits are shown with the solid lines.

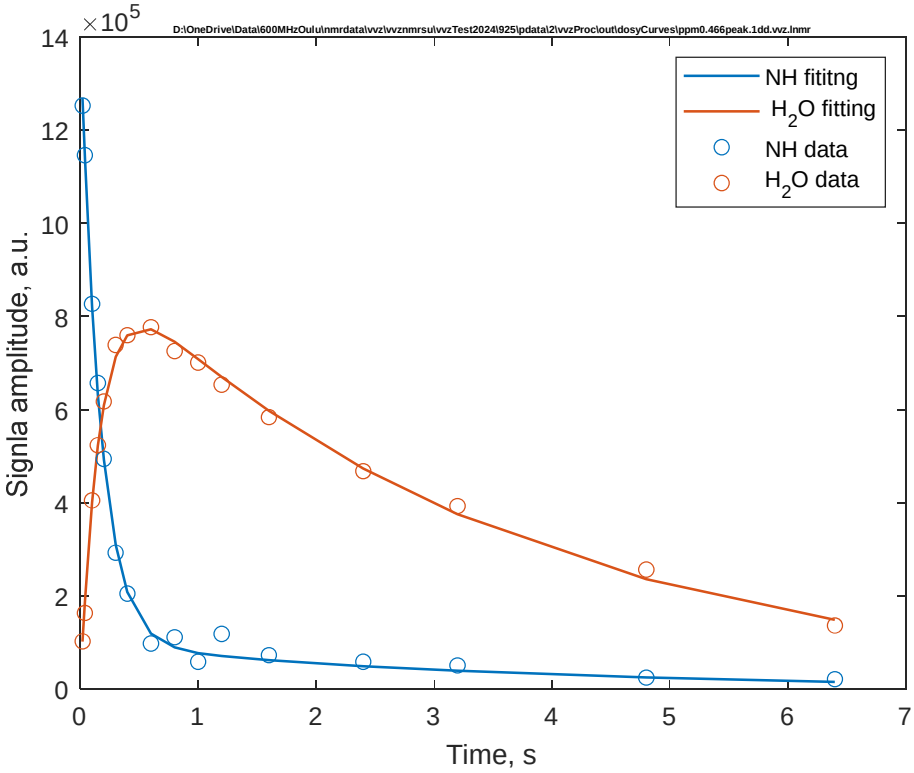

Figure S10. Kinetic curves obtained from 1D EXSY ^{1}H NMR for **MesCAT-H$_2$O** at 286 K in toluene-d8. The integral data points for NH and H_2O signals are shown with circles (see legend). The corresponding least-squares fits are shown with the solid lines.

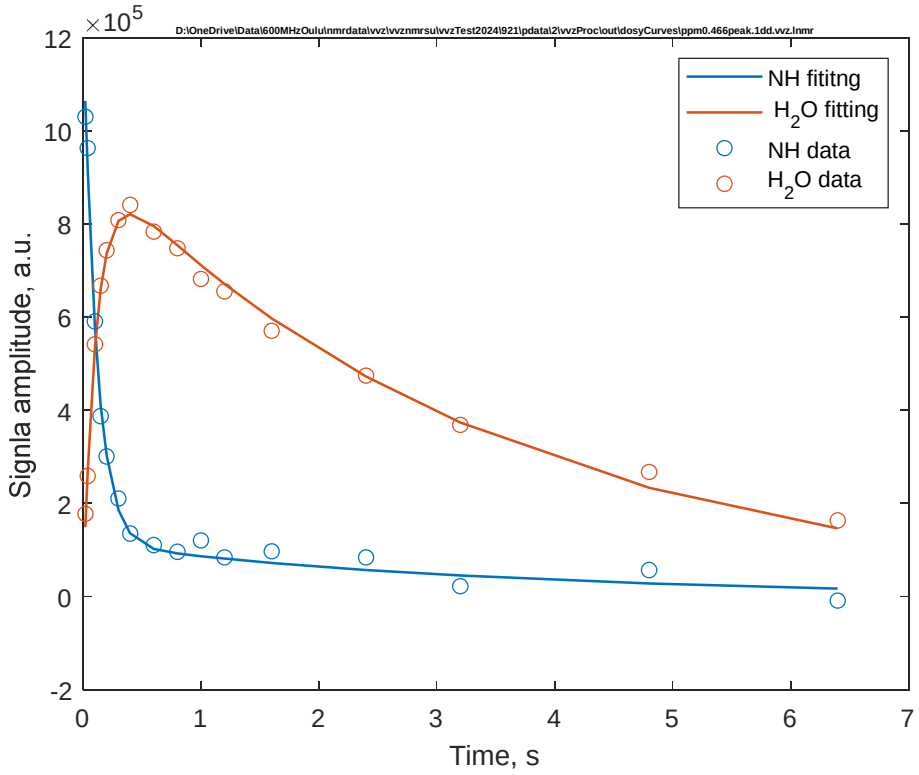

Figure S11. Kinetic curves obtained from 1D EXSY ^{1}H NMR for **MesCAT-H$_2$O** at 290 K in toluene-d8. The integral data points for NH and H_2O signals are shown with circles (see legend). The corresponding least-squares fits are shown with the solid lines.

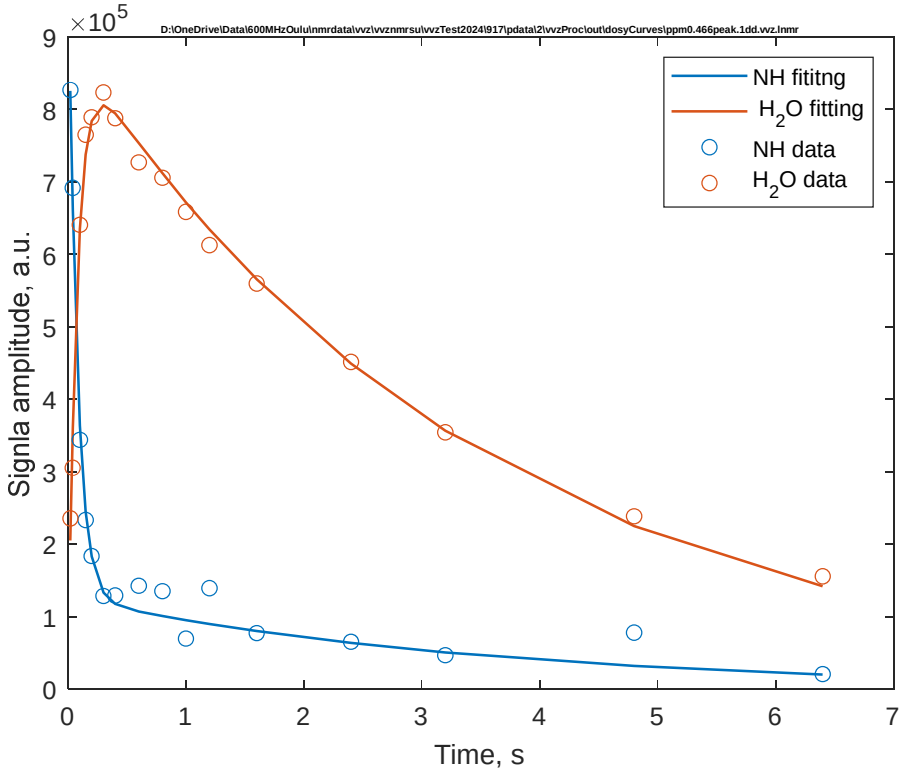

Figure S12. Kinetic curves obtained from 1D EXSY ^{1}H NMR for **MesCAT-H$_2$O** at 294 K in toluene-d8. The integral data points for NH and H_2O signals are shown with circles (see legend). The corresponding least-squares fits are shown with the solid lines.

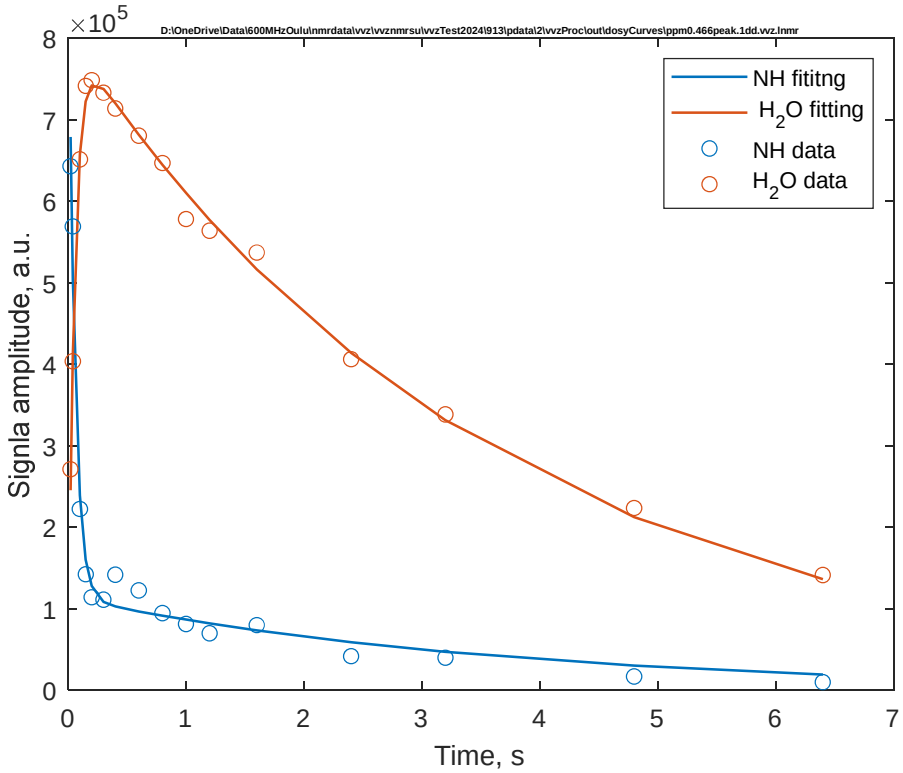

Figure S13. Kinetic curves obtained from 1D EXSY ^{1}H NMR for **MesCAT-H$_2$O** at 297 K in toluene-d8. The integral data points for NH and H_2O signals are shown with circles (see legend). The corresponding least-squares fits are shown with the solid lines.

1.6.3 Dissociation constants for MesCAT-H$_2$O water adduct in acetonitrile-d3 and toluene-d8 at various temperatures

The experimentally measured dissociation constants from EXSY NMR for **MesCAT-H$_2$O** in acetonitrile-d3 and toluene-d8 at various temperatures are shown in the table below.

Table S1. Experimentally measured dissociation rates for **MesCAT-H$_2$O** in acetonitrile and toluene.

Solvent	Temperature, (K)	k'_{dis}, 1/s
ACN	294	1.6±0.1
	298	2.7±0.2
	302	4.0±0.4
	302	3.8±0.3
	306	6.8±0.6
	306	6.4±0.4
TOL	296.8	15±1
	294	11.3±0.6
	290	6.5±0.3
	286	3.8±0.1

TOL = toluene; ACN = acetonitrile.

To find the dissociation rates for the temperatures used in the parahydrogen experiments, an interpolation was performed using the Arrhenius equation,

$$k'_{\mathrm{dis}} = A \exp\left(-\frac{E_{\mathrm{a}}}{RT}\right), \qquad \text{(S1)}$$

where A is a pre-exponential factor, E_{a} is an activation energy, and R is the universal gas constant. The A and E_{a} parameters were obtained from fitting the Arrhenius equation to the experimentally measured values of rate constants from the variable temperature EXSY NMR measurements.

1.7 Discussion on the influence of the MesCAT ÷ H_2O ratio on PHIP observations

Even though in this initial communication we do not consider the variation of water concentration on the observed hyperpolarization in details, it is possible to provide a general discussion on these matters, setting a perspective for the future studies.

To assess the influence of water concentration, it is important to realize that the major effect of the presence of moisture in MesCAT solutions is temporary trapping of active MesCAT species in the form of inactive MesCAT-H_2O adduct. In other words, the moisture present in the solution decreases the equilibrium concentration of hyperpolarized MesCAT-H_2 species, effectively decreasing the absolute amplitudes of hyperpolarized ^{1}H NMR signals. The drop in the equilibrium concentration of MesCAT-H_2 can be obtained by defining the equilibrium constant for hydrogen activation by MesCAT (K_{c}) and hydration of MesCAT (K'_{c}):

$$\mathrm{MesCAT} + \mathrm{H_2} \rightleftharpoons \mathrm{MesCAT{-}H_2}, \qquad K_{\mathrm{c}} = \frac{[\mathrm{MesCAT{-}H_2}]}{[\mathrm{MesCAT}][\mathrm{H_2}]} \qquad \text{(eq S5)}$$

$$\mathrm{MesCAT} + \mathrm{H_2O} \rightleftharpoons \mathrm{MesCAT{-}H_2O}, \qquad K'_{\mathrm{c}} = \frac{[\mathrm{MesCAT{-}H_2O}]}{[\mathrm{MesCAT}][\mathrm{H_2O}]}. \qquad \text{(eq S6)}$$

Following our experimental protocol, the total concentration of MesCAT derived species, defined as

$$\Sigma_{\mathrm{MesCAT}} = [\mathrm{MesCAT}] + [\mathrm{MesCAT{-}H_2}] + [\mathrm{MesCAT{-}H_2O}], \qquad \text{(eq S7)}$$

is equal to the initial concentration of [MesCAT-H_2]$_0$. Two cases can be considered at this point as described below.

Case 1: We have a significant excess of water so that [H_2O]$_0$ >> [MesCAT-H_2] + [MesCAT-H_2], where [H_2O]$_0$ is the initial water concentration in the water-containing solvent and [H_2O] is the equilibrium concentration. In this case we can assume that [H_2O] ≈ [H_2O]$_0$. This is the case we deal with in the paper. By noting that the equilibrium concentration of MesCAT-H_2O is equal to

$$[\mathrm{MesCAT{-}H_2O}] = [\mathrm{MesCAT{-}H_2O}]_0 - [\mathrm{MesCAT}] - [\mathrm{MesCAT{-}H_2}], \qquad \text{(eq S8)}$$

and substituting this expression in eq S6 followed by solving the resulting equation system (eq S5 and S6) with respect to [MesCAT] and [MesCAT-H_2] it is possible to show that

$$[\mathrm{MesCAT}] = \frac{\Sigma_{\mathrm{MesCAT}}}{1 + K_c[\mathrm{H_2}] + K_c'[\mathrm{H_2O}]}, \qquad \text{(eq S9)}$$

$$[\mathrm{MesCAT{-}H_2}] = \frac{K_c[\mathrm{H_2}]\Sigma_{\mathrm{MesCAT}}}{1 + K_c[\mathrm{H_2}] + K_c'[\mathrm{H_2O}]}. \qquad \text{(eq S10)}$$

Finally, by defining the ratio of the concentration of the MesCAT forms to water concentration as

$$\xi = \frac{\Sigma_{\mathrm{MesCAT}}}{[\mathrm{H_2O}]}, \qquad \text{(eq S11)}$$

we find that

$$[\mathrm{MesCAT{-}H_2}] = \frac{K_c[\mathrm{H_2}]}{\frac{1}{\Sigma_{\mathrm{MesCAT}}} + \frac{K_c[\mathrm{H_2}]}{\Sigma_{\mathrm{MesCAT}}} + \frac{K_c'}{\xi}}. \qquad \text{(eq S12)}$$

This expression shows that by decreasing the MesCAT ÷ H_2O ratio reflected by ξ, the equilibrium concentration of MesCAT-H_2 decreases, leading to a lower absolute concentration of hyperpolarized MesCAT-H_2 species.

Case 2: The $[H_2O]_0$ and [MesCAT-H_2] + [MesCAT-H_2] concentrations are comparable. In this case we cannot assume that $[H_2O]_0 \approx [H_2O]$ and we need to solve the set of eq S5 and S6 by taking [MesCAT-H_2O] from eq S8 and [H_2O] from

$$[\mathrm{H_2O}] = [\mathrm{H_2O}]_0 + [\mathrm{MesCAT}] + [\mathrm{MesCAT{-}H_2}]. \qquad \text{(eq S13)}$$

In this case, the formula for [MesCAT-H_2] is significantly less compact and reads as

$$[\mathrm{MesCAT{-}H_2}] = \frac{K_c[\mathrm{H_2}]\sqrt{(1 + K_c[\mathrm{H_2}] + K_c'[\mathrm{H_2O}])^2 + 4K_c'\Sigma_{\mathrm{MesCAT}}(1 + K_c[\mathrm{H_2}])}}{2(K_c' + K_cK_c'[\mathrm{H_2}])} - \frac{K_c[\mathrm{H_2}](1 + K_c[\mathrm{H_2}] + K_c'[\mathrm{H_2O}])}{2(K_c' + K_cK_c'[\mathrm{H_2}])}. \qquad \text{(eq S14)}$$

It is difficult to find the compact form for this case with the MesCAT ÷ H_2O ratio included as well (ξ, eq S11), but generally this expression is also implying that the increase of water concentration decreases the concentration of hyperpolarized MesCAT-H_2 species and describes the thermodynamic equilibria more precisely at low water concentrations.

Clearly, Case 2 is more complex than Case 1 touched on in this communication. The detailed study of the thermodynamics of water addition is beyond the scope of this work and will be addressed in future studies in detail.

We note that, as a good approximation, it is true that neither H_2O nor MesCAT-H_2O lead to the conversion of para-H_2 into ortho-H_2, and essentially, they act as spectator molecules in the context of hyperpolarization. The main influence of H_2O is in changing the concentration of the hyperpolarized MesCAT-H_2 species. However, as the first approximation, the presence of H_2O does not change signal enhancements directly by an involvement in the para-H_2 activation process, since signal enhancements are relative quantities defined as the ratios of amplitudes of hyperpolarized and thermal signals of MesCAT-H_2. However, the change in the equilibrium concentration of MesCAT-H_2 can indirectly influence the observed signal enhancement through the changed MesCAT-H_2 ÷ para-H_2 ratio. Lower MesCAT-H_2 ÷ para-H_2 ratios can lead to stronger signal enhancements which was shown experimentally and using a rigorous density matrix theoretical consideration described for various AABs in our recent publication.[S5] In particular, it was shown that by decreasing AAB concentration and keeping para-H_2 concentration, one can significantly increase the observed signal enhancements for AAB-H_2 adducts. Even though, for MesCAT this effect is less pronounced due to thermodynamic factors (relatively low K_c constant), in the context of the presence of moisture, it would mean that by adding water one can decrease the AAB-H_2 concentration, and through that increase the MesCAT-H_2 ÷ para-H_2 ratio. Finally, this should lead to the stronger relative signal enhancements but lower total concentration of the hyperpolarized species. The effect is not linear and deserves further investigation in the future.

2 Computational details

All DFT calculations were carried out using *Gaussian16*.[S7] The ωB97X-D[S8] functional was chosen as this dispersion-corrected, range-separated hybrid method was found to describe hydrogen activation via FLP accurately. All structures were optimized in the gas phase at the ωB97X-D/6-311G** level. Thermal and entropic corrections were calculated at the same level of theory and within Grimme's quasi-RRHO approximation.[S9] The solvation Gibbs free energy was calculated also at the ωB97X-D/6-311G** level using the gas-phase structures and the SMD implicit solvation model.[S10] The electronic energies were recalculated at the ωB97X-D/6-311++G(3df,3pd) level of theory. The final Gibbs free energies were calculated according to the following formula:

$$G = E_0' + (G_0 - E_0) + (G_{sol} - E_0) + \Delta G_{conc}, \qquad \text{(eq S15)}$$

where E_0 and E_0' refer to electronic energies computed at the ωB97X-D/6-311G** and the ωB97X-D/6-311++G(3df,3pd) levels of DFT, respectively; G_0 denotes the gas-phase Gibbs free energy; G_{sol} is the energy in solution-phase. ΔG_{conc} refers to the concentration correction (all Gibbs free energies were computed at the temperature of 298.15 K and were corrected to the 1 mol/dm^3 concentration).

The calculation covered "a" and "b" forms of **MesCAT** and **PhCAT** derivatives, such as water and dihydrogen adducts. These forms are differing by the conformation of the TMP substituent.[S5] The geometries of the most stable species are shown in the main text. The tables below list Gibbs free energies obtained in the DFT modelling for AAB-H_2O + H_2 and AAB-H_2 + H_2O levels to compare the thermodynamic stabilities of water and dihydrogen adducts, respectively.

Table S2. Gibbs free energies for the comparison of stabilities of water and dihydrogen adducts of **MesCAT**.

State	TOL, Hartree	ACN, Hartree	[a]TOL, kcal/mol	[a]ACN, kcal/mol
MesCAT-H_2O-a + H_2	-1440.660907	-1440.668346	6.7	2.0
MesCAT-H_2-a + H_2O	-1440.655798	-1440.668960	9.9	1.6
MesCAT-H_2O-b + H_2	-1440.662513	-1440.669102	5.7	1.5
MesCAT-H_2-b + H_2O	-1440.659196	-1440.671549	7.8	0.0

[a]The energies are shown with respect to the most stable form. TOL = toluene; ACN = acetonitrile.

Table S3. Gibbs free energies for the comparison of stabilities of water and dihydrogen adducts of **PhCAT**.

State	TOL, Hartree	ACN, Hartree	[a]TOL, kcal/mol	[a]ACN, kcal/mol
PhCAT-H_2O-a + H_2	-1204.939930	-1204.948346	5.3	0.0
PhCAT-H_2-a + H_2O	-1204.924256	-1204.938528	15.1	6.2
PhCAT-H_2O-b + H_2	-1204.938206	-1204.946052	6.4	1.4
PhCAT-H_2-b + H_2O	-1204.923882	-1204.937472	15.4	6.8

[a]The energies are shown with respect to the most stable form. TOL = toluene; ACN = acetonitrile.

2.1 XYZ coordinates of the optimized structures

The structures of **MesCAT-H$_2$-a**, **MesCAT-H$_2$-b**, **PhCAT-H$_2$-a**, and **MesCAT-H$_2$-b** are published in Ref.[S5] The coordinates for all other structures optimized in this work are listed below. All structures are well-defined minima with positive lowest frequencies (see section titles below).

2.1.1 H_2 (Lowest frequency: 4435.1250 cm^{-1})

2
/drives/d/ExpDir/SchrodingerProjects/MesCAT-H2O/GaussianH2:H2.log
H 0.757126 2.871550 0.000000
H 0.012726 2.871550 -0.000000

2.1.2 H_2O (Lowest frequency: 1640.9058 cm^{-1})

3
/drives/d/ExpDir/SchrodingerProjects/MesCAT-H2O/GaussianH2O:H2O.log
O -0.000000 -0.033952 0.000000
H 0.755106 0.554275 -0.000000
H -0.755106 0.554275 0.000000

2.1.3 MesCAT-H$_2$O-a (Lowest frequency: 15.1141 cm^{-1})

82
/drives/d/ExpDir/SchrodingerProjects/MesCAT-H2O/GaussianMesCATaH2O:MesCATaH2O.log
C -2.380198 -0.813215 2.388087
C -1.681712 -0.573132 1.208129
C -0.273680 -0.580561 1.137848
C 0.356810 -1.030672 2.307683
C -0.319076 -1.306439 3.485270
C -1.696569 -1.151130 3.544804
N -2.443655 -0.439202 -0.058476
C -3.297318 0.822518 -0.278516
C -3.614436 0.865878 -1.784000
C -4.228958 -0.413750 -2.336198
C -3.316724 -1.600408 -2.049268
C -3.018852 -1.790674 -0.554679
C -2.434901 2.034483 0.065559
C -4.574073 0.903765 0.559689
C -1.928892 -2.851225 -0.386031
C -4.261861 -2.285961 0.188140
B 0.669556 -0.044511 -0.133836
C 2.036631 -1.007262 -0.246916
C 1.040931 1.588400 -0.095276
H -3.758411 -2.527998 -2.423068
H -2.364528 -1.465425 -2.573937
H -2.682036 1.073641 -2.320944
H -4.273467 1.720440 -1.959092
H -5.223933 -0.578422 -1.910482
H -4.371979 -0.312654 -3.414982
H -1.456770 1.994308 -0.411936
H -2.286851 2.127889 1.140919

H	-2.947381	2.934215	-0.282695
H	-5.027943	1.877206	0.358679
H	-4.358366	0.869947	1.626953
H	-5.316165	0.146096	0.323343
H	-1.800615	-3.136840	0.658801
H	-0.972046	-2.507584	-0.767343
H	-2.226411	-3.737146	-0.952504
H	-4.455284	-3.302269	-0.163565
H	-5.160495	-1.705456	-0.003689
H	-4.098392	-2.347718	1.262665
H	-3.458966	-0.762694	2.410004
H	-2.241155	-1.330557	4.464429
H	0.231898	-1.633132	4.360335
H	1.431038	-1.162558	2.290662
H	-1.631159	-0.276120	-0.744127
O	-0.269195	-0.170790	-1.354923
C	2.149874	-2.151411	-1.072992
C	3.284309	-2.971087	-1.033601
C	4.361755	-2.717110	-0.209731
C	4.289255	-1.569731	0.568493
C	3.182971	-0.724803	0.553976
C	1.655395	2.122377	-1.256344
C	1.935594	3.485172	-1.377733
C	1.630336	4.391267	-0.378690
C	1.051737	3.878423	0.773636
C	0.766026	2.523519	0.938855
H	0.824793	4.561176	1.588937
H	2.416493	3.840774	-2.286292
H	5.133351	-1.313614	1.204344
H	3.313653	-3.839779	-1.688472
C	1.135351	-2.608147	-2.108184
H	0.684534	-3.561107	-1.810321
H	0.347657	-1.884985	-2.277195
C	5.558229	-3.629441	-0.151476
H	5.547707	-4.231539	0.763016
H	5.575483	-4.316311	-1.000844
C	3.329010	0.512809	1.415452
H	3.499852	1.403104	0.806209
H	2.451466	0.714779	2.024618
C	1.902451	5.864662	-0.530225
H	0.992519	6.405071	-0.811707
H	2.264914	6.299315	0.404945
C	2.072836	1.287528	-2.457304
H	2.284023	0.250739	-2.207198
H	1.312816	1.302844	-3.251034
C	0.215677	2.168648	2.306119
H	-0.664752	1.533095	2.277174
H	0.954133	1.637869	2.912817
H	6.491794	-3.060079	-0.156616

H 4.179698 0.398960 2.091551
H 1.646431 -2.788542 -3.059103
H 2.650881 6.052155 -1.303597
H 2.976351 1.709528 -2.902761
H -0.046970 3.080266 2.847525
H -0.043614 0.472651 -2.023976

2.1.4 MesCAT-H_2O-b (Lowest frequency: 23.9672 cm^{-1})

82
/drives/d/ExpDir/SchrodingerProjects/MesCAT-H2O/GaussianMesCATbH2O:MesCATbH2O.log
O 0.198610 -0.587335 -1.529699
H 0.700050 -0.388100 -2.316256
B 0.897660 -0.033279 -0.296767
C 0.122596 -0.900073 0.918702
C 0.846627 -1.414586 2.007956
H 1.919332 -1.255918 2.017878
C 0.272074 -2.122405 3.047899
H 0.890512 -2.494165 3.857370
C -1.098912 -2.352921 3.050497
H -1.573604 -2.893450 3.861072
C -1.853938 -1.897151 1.986530
H -2.916296 -2.094638 1.972089
C -1.244236 -1.204164 0.941683
N -2.091263 -0.812218 -0.223427
H -1.386485 -0.395479 -0.868347
C -2.594984 -2.033587 -1.073135
C -3.958210 -2.528735 -0.581799
H -4.289324 -3.286847 -1.297582
H -3.835607 -3.048114 0.372698
C -5.004364 -1.432974 -0.443450
H -5.931707 -1.855206 -0.048199
H -5.254449 -1.013068 -1.422215
C -4.498393 -0.345907 0.491927
H -4.417212 -0.744754 1.507214
H -5.219466 0.474544 0.548772
C -3.158312 0.284644 0.088098
C -3.320113 1.177574 -1.148158
H -3.875909 0.711300 -1.957827
H -2.349421 1.507918 -1.519141
H -3.868199 2.072820 -0.848948
C -2.675748 1.173069 1.233435
H -1.747083 1.679534 0.983198
H -2.535812 0.619975 2.161159
H -3.441404 1.933609 1.403696
C -1.574043 -3.167212 -0.986849
H -0.604934 -2.823916 -1.340750
H -1.923004 -3.977115 -1.631944
H -1.465584 -3.561244 0.022659
C -2.669857 -1.604745 -2.546501

H -3.522661 -0.971845 -2.777709
H -2.763290 -2.506737 -3.154160
H -1.752483 -1.095571 -2.842979
C 0.498684 1.579382 -0.114657
C 0.052625 2.374684 -1.197178
C -0.448108 3.663124 -0.992812
H -0.791822 4.234061 -1.852554
C -0.484797 4.254669 0.260236
C 0.068210 3.531339 1.307119
H 0.129520 3.989749 2.291531
C 0.554324 2.236227 1.138834
C 1.181237 1.610148 2.362692
H 1.535537 2.391150 3.040137
H 2.033870 0.981561 2.103900
H 0.469665 0.990310 2.913989
C -1.068528 5.626335 0.471888
H -1.048537 6.213844 -0.449106
H -0.518207 6.177573 1.238423
H -2.111486 5.562311 0.800228
C 0.180057 1.962524 -2.652845
H -0.581438 1.245215 -2.969113
H 1.161525 1.521483 -2.852245
H 0.092805 2.841906 -3.294971
C 2.523006 -0.377021 -0.378002
C 2.939127 -1.732795 -0.510247
C 4.284591 -2.091203 -0.481917
H 4.549901 -3.141898 -0.572032
C 5.296758 -1.151208 -0.355780
C 4.911757 0.176203 -0.312860
H 5.682377 0.941641 -0.267906
C 3.571073 0.578585 -0.338233
C 3.382197 2.083403 -0.366958
H 4.341808 2.565086 -0.567906
H 3.007738 2.483998 0.575973
H 2.685206 2.400965 -1.140691
C 6.743540 -1.560756 -0.275984
H 7.009887 -1.854851 0.744696
H 7.405153 -0.741331 -0.566590
H 6.951813 -2.413800 -0.927148
C 1.978055 -2.877355 -0.747740
H 1.520694 -2.793558 -1.735892
H 1.168964 -2.908740 -0.020817
H 2.506754 -3.832281 -0.702591

2.1.5 **PhCAT-H_2O-a** (Lowest frequency: 19.7367 cm^{-1})

64
/drives/d/ExpDir/SchrodingerProjects/MesCAT-H2O/GaussianPhCATaH2O:PhCATaH2O.log
C 1.891912 -0.268920 2.402062
C 1.194300 -0.190772 1.197417

C	-0.203289	-0.230932	1.119758
C	-0.857364	-0.383545	2.352796
C	-0.188731	-0.464642	3.562558
C	1.199031	-0.400208	3.592738
N	1.947820	-0.101812	-0.075471
C	2.657455	1.240512	-0.344027
C	3.053507	1.234308	-1.829557
C	3.844463	0.004333	-2.255272
C	3.032558	-1.252199	-1.967667
C	2.654611	-1.413613	-0.487491
C	1.627716	2.348508	-0.115367
C	3.866777	1.522844	0.547696
C	1.630143	-2.543744	-0.355289
C	3.877388	-1.782241	0.353615
B	-1.141319	-0.043173	-0.230394
C	-2.279637	-1.207827	-0.332038
C	-1.845458	1.435323	-0.248740
H	3.578494	-2.148903	-2.272402
H	2.107254	-1.225868	-2.553693
H	2.137404	1.290677	-2.428132
H	3.615894	2.150590	-2.027464
H	4.812214	-0.031532	-1.744538
H	4.064023	0.063160	-3.324240
H	0.714740	2.180463	-0.686145
H	1.354372	2.434793	0.936855
H	2.063881	3.297572	-0.435463
H	4.244371	2.511442	0.275773
H	3.589312	1.565375	1.599994
H	4.685979	0.818537	0.424241
H	1.391770	-2.755175	0.687748
H	0.705395	-2.304134	-0.877503
H	2.057700	-3.445465	-0.800231
H	4.241549	-2.743913	-0.015833
H	4.700984	-1.076106	0.278976
H	3.619997	-1.920532	1.402533
H	2.971380	-0.232722	2.420295
H	1.739224	-0.459411	4.530393
H	-0.748795	-0.579445	4.484048
H	-1.939612	-0.440856	2.354374
H	1.146867	-0.059930	-0.784658
O	-0.212017	-0.148645	-1.450497
C	-2.100574	-2.340603	-1.132625
C	-3.056106	-3.348777	-1.214351
C	-4.237194	-3.249448	-0.490584
C	-4.456327	-2.123419	0.294872
C	-3.495237	-1.121798	0.360470
C	-2.640467	1.776725	-1.353573
C	-3.236812	3.024593	-1.482093
C	-3.068503	3.980047	-0.485688

C -2.304897 3.665980 0.630499
C -1.705220 2.414144 0.739639
H -3.536733 4.954426 -0.574859
H -2.174385 4.398345 1.421046
H -1.111009 2.198390 1.622744
H -2.823608 1.030262 -2.124490
H -3.846089 3.248544 -2.351898
H -3.709023 -0.231423 0.946403
H -5.385251 -2.019445 0.846627
H -4.985926 -4.032236 -0.549592
H -2.880302 -4.211819 -1.849169
H -1.198534 -2.422546 -1.730560
H -0.559819 0.368824 -2.175485

2.1.6 PhCAT-H_2O-b (Lowest frequency: 27.1834 cm^{-1})

64
/drives/d/ExpDir/SchrodingerProjects/MesCAT-H2O/GaussianPhCATbH2O:PhCATbH2O.log
B -1.251246 -0.024586 -0.273851
O -0.461759 -0.176262 -1.580429
C -0.309168 -0.547814 0.983530
C -0.925254 -0.923435 2.188982
H -2.009856 -0.939101 2.223507
C -0.211936 -1.284249 3.319774
H -0.736343 -1.564319 4.226764
C 1.178536 -1.290500 3.288140
H 1.752646 -1.566807 4.164869
C 1.829350 -0.946020 2.116566
H 2.909956 -0.954645 2.089776
C 1.085260 -0.590533 0.993922
N 1.776945 -0.230214 -0.270623
H 0.955309 -0.112826 -0.931353
C 2.533239 -1.408993 -0.940688
C 3.974559 -1.491221 -0.430765
H 3.981394 -1.865659 0.596229
H 4.486019 -2.247927 -1.033336
C 4.719007 -0.161574 -0.506742
H 4.876547 0.127549 -1.550034
H 5.715230 -0.275442 -0.072042
C 3.962590 0.933528 0.237034
H 4.470946 1.894196 0.114037
H 3.972296 0.721654 1.310416
C 2.510781 1.134744 -0.216193
C 1.798894 2.065374 0.770498
H 0.763873 2.247640 0.480127
H 2.327534 3.021408 0.758514
H 1.811505 1.683590 1.790375
C 2.424097 1.795918 -1.598962
H 1.399633 1.762793 -1.976386
H 3.088195 1.355954 -2.339257

H	2.704474	2.845290	-1.492570
C	1.774789	-2.705139	-0.638545
H	0.740890	-2.635680	-0.983371
H	1.766831	-2.951239	0.421923
H	2.264755	-3.519076	-1.177223
C	2.516705	-1.220287	-2.468185
H	1.536804	-0.895225	-2.818658
H	2.740367	-2.183291	-2.930743
H	3.262313	-0.514104	-2.824763
C	-2.594348	-0.933742	-0.401382
C	-3.861429	-0.386060	-0.625695
C	-4.983376	-1.187211	-0.816059
C	-4.867031	-2.571357	-0.790942
C	-3.620627	-3.146052	-0.568558
C	-2.509685	-2.333827	-0.374780
C	-1.558302	1.566038	-0.087648
C	-1.448782	2.438549	-1.176309
C	-1.674299	3.806442	-1.051785
C	-2.028051	4.344853	0.178693
C	-2.162459	3.498752	1.274426
C	-1.930672	2.135490	1.136470
H	-2.027970	1.502105	2.013310
H	-2.445073	3.904692	2.240648
H	-2.202322	5.410460	0.283536
H	-1.575610	4.453100	-1.918323
H	-1.171558	2.025925	-2.140833
H	-3.971113	0.693862	-0.649464
H	-5.952633	-0.728851	-0.984649
H	-5.740392	-3.197848	-0.938071
H	-3.518075	-4.226252	-0.537907
H	-1.548090	-2.802220	-0.173341
H	-0.851145	-0.875226	-2.103447

3 Full-range ^{1}H and ^{11}B NMR spectra from the experiments with MesCAT-H_2O and PhCAT-H_2O

3.1 NMR spectra from the experiments with parahydrogen and MesCAT-H_2O

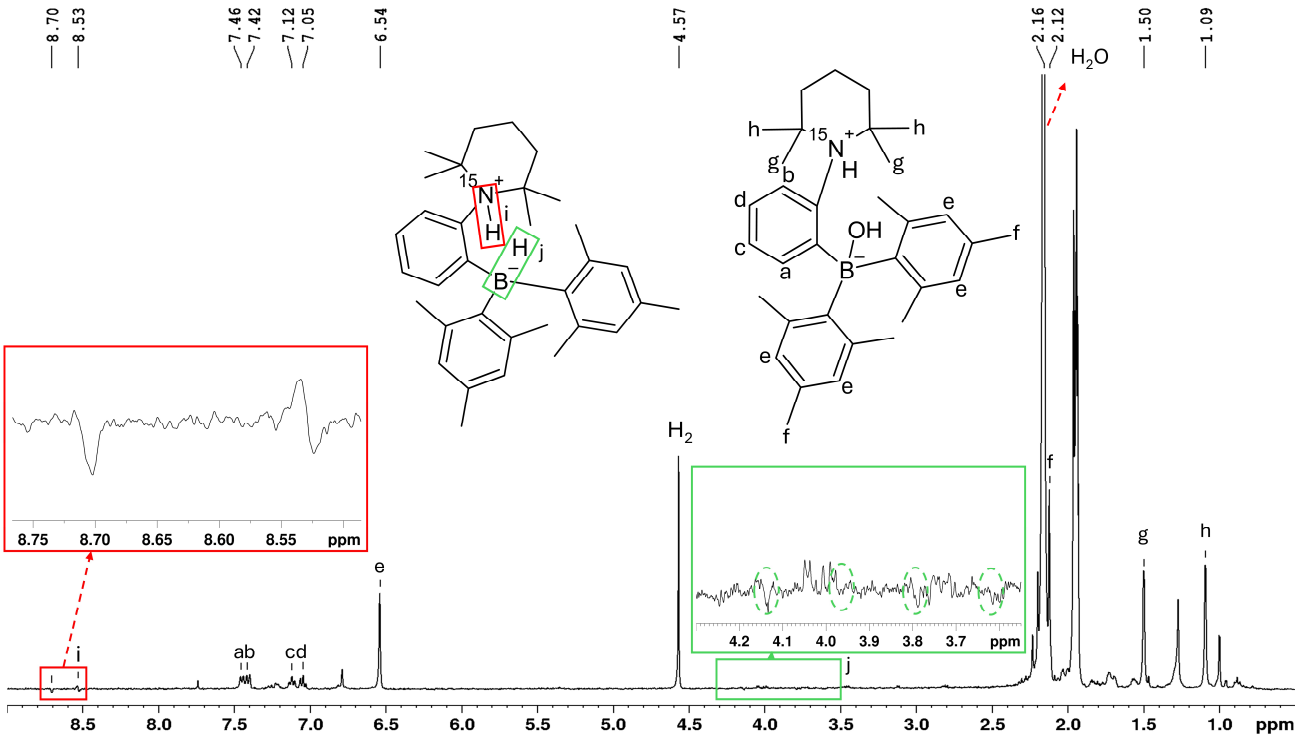

Figure S14. ^{1}H NMR spectrum of a 1 mM solution of MesCAT-H_2O, parahydrogen (6 bars), and 100 equivalents of H_2O in acetonitrile-d3 at 297 K with assignments of the signals. The inset with the red frame shows the antiphase signals (two antiphase doublets) corresponding to the ^{15}N-H group proton (i) of the hyperpolarized **MesCAT-H_2**, which was generated in the solution. The inset with the green frame shows the range where the ^{11}B-H group proton should be visible. Due to the low signal-to-noise ratio, the latter was difficult to detect at this temperature with 8 scan accumulations, but with 128 scans it was visible more clearly (see the next figure).

Number of accumulations (NS parameter): 8
^{1}H NMR (400.13 MHz, acetonitrile-d3):
MesCAT-H_2O, δ**:** a) 7.46 (d, *J* = 7.72 Hz, 1H); b) 7.42 (d, *J* = 8.16 Hz, 1H); c) 7.14 (t, *J* = 7.40 Hz; 1H); d) 7.06 (t, *J* = 7.04 Hz, 1H); e) 6.54 (s, 4H); f) 2.12 (s, 6H); g) 1.50 (s, 6H); h) 1.09 (s, 6H),
Water, δ: 2.16 (s, 2H),
H_2, δ: 4.57 (s, 2H),
MesCAT-H_2, δ: i) 8.63 (dd, ^{HH}J = 3.92 Hz, ^{HN}J = 71.56 Hz, 1H) ppm.

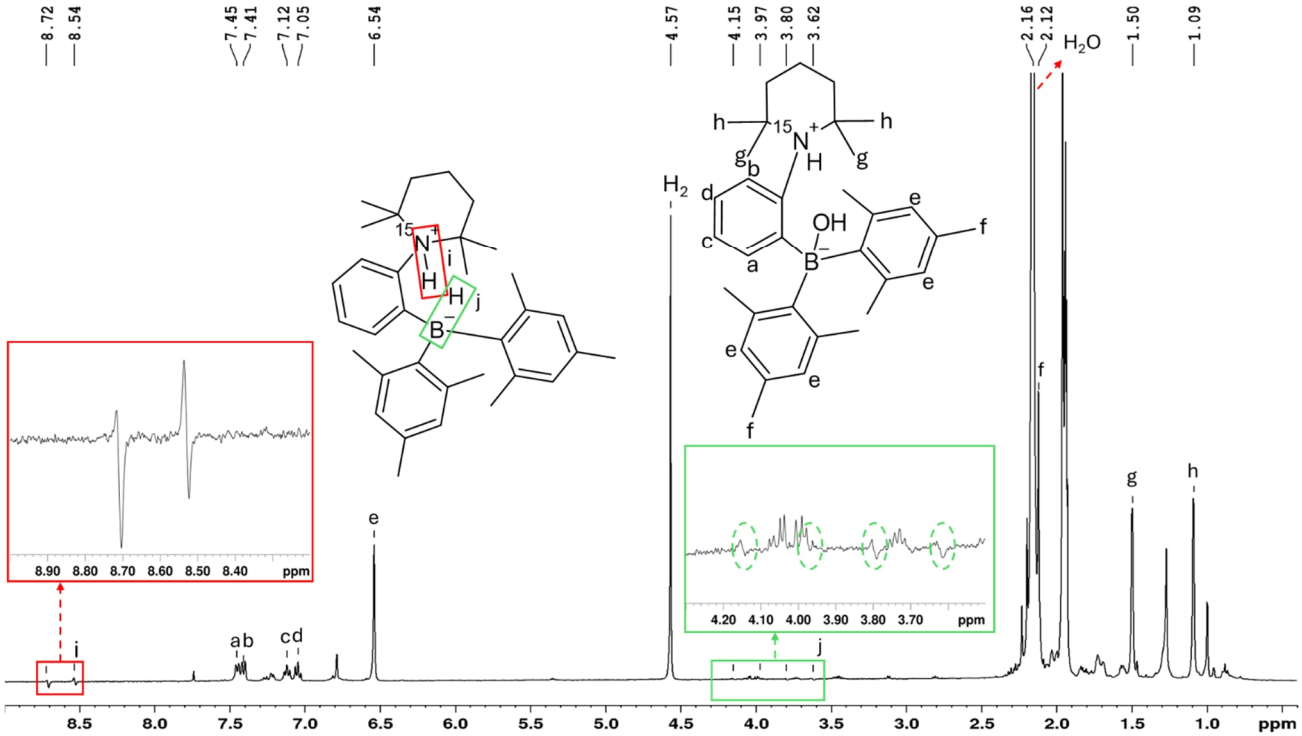

Figure S15. ^{1}H NMR spectrum of a 1 mM solution of MesCAT-H_2O, parahydrogen (6 bars), and 100 equivalents of H_2O in acetonitrile-d3 at 297 K with assignments of the signals. A bigger number of scan accumulations (NS = 128) was used in this case as compared to the previous figure (NS = 8). The insets show the antiphase signals corresponding to the ^{15}N-H group (red, two antiphase doublets) and the ^{11}B-H group (green, four antiphase doublets) protons of the hyperpolarized **MesCAT-H$_2$**, which was generated in the solution.

Number of accumulations (NS parameter): 128
^{1}H NMR (400.13 MHz, acetonitrile-d3):
MesCAT-H$_2$O, δ**:** a) 7.46 (d, *J* = 7.72 Hz, 1H); b) 7.42 (d, *J* = 8.16 Hz, 1H); c) 7.14 (t, *J* = 7.40 Hz; 1H); d) 7.06 (t, *J* = 7.04 Hz, 1H); e) 6.54 (s, 4H); f) 2.12 (s, 6H); g) 1.50 (s, 6H); h) 1.09 (s, 6H),
Water, δ: 2.16 (s, 2H),
H$_2$, δ: 4.57 (s, 2H),
MesCAT-H$_2$, δ: i) 8.63 (dd, ^{HH}J = 3.92 Hz, ^{HN}J = 71.56 Hz, 1H) ppm.

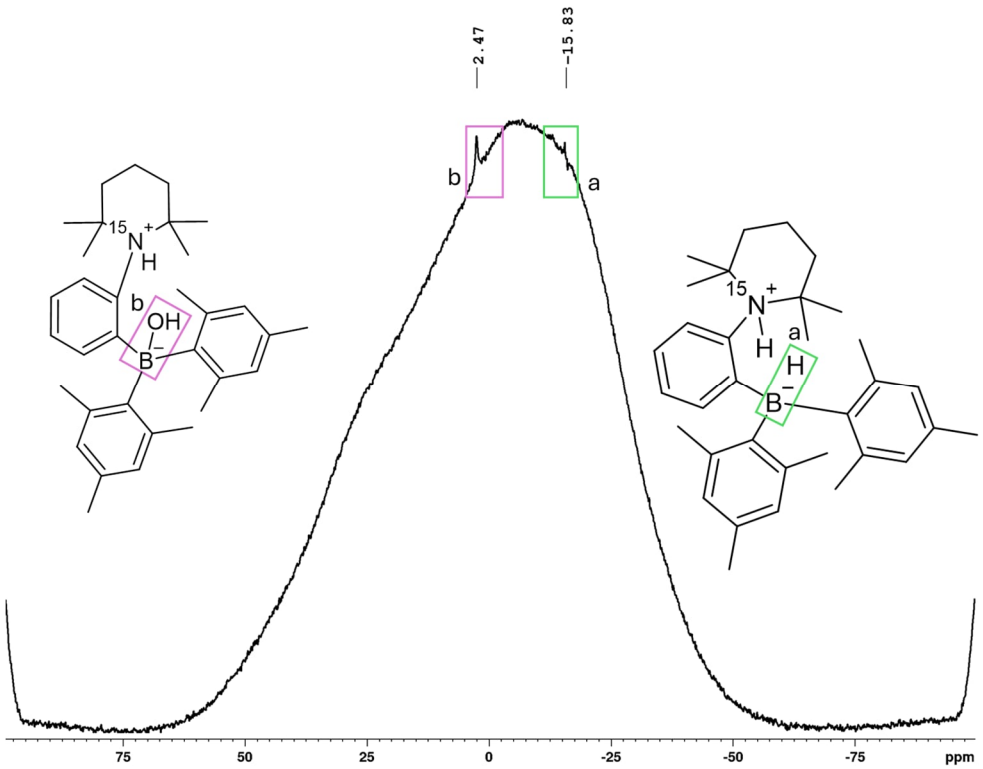

Figure S16. ^{11}B NMR spectrum of a 1 mM solution of MesCAT-H_2O, parahydrogen (6 bars), and 100 equivalents of H_2O in acetonitrile-d3 at 297 K with assignments of the signals. The antiphase signal marked with a green rectangle corresponds to the hyperpolarized **MesCAT-H_2** which was generated in the solution.

Number of accumulations (NS parameter): 256
^{11}B NMR (128.38 MHz, acetonitrile-d3):
MesCAT-H_2, δ: a) -15.83 (d, ^{BH}J = 71.5 Hz, 1B),
MesCAT-H_2O, δ: b) 2.47 (s, 1B) ppm.

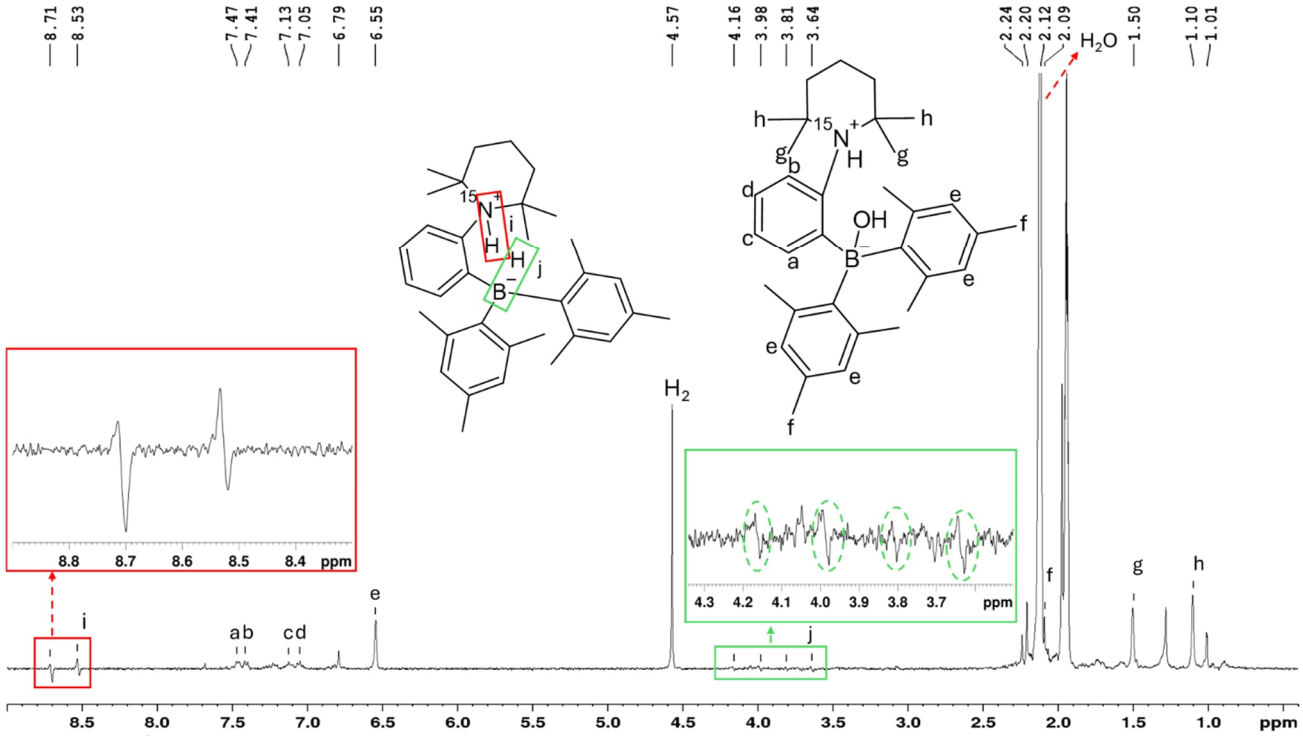

Figure S17. ^{1}H NMR spectrum of a 1 mM solution of MesCAT-H_2O, parahydrogen (6 bars), and 100 equivalents of H_2O in acetonitrile-d3 at 308 K with assignments of the signals. The insets show the antiphase signals corresponding to the ^{15}N-H group (red, two antiphase doublets) and the ^{11}B-H group (green, four antiphase doublets) protons of the hyperpolarized **MesCAT-H_2**, which was generated in the solution.

Number of accumulations (NS parameter): 1
^{1}H NMR (400.13 MHz, acetonitrile-d3):
MesCAT-H_2O, δ: a) 7.47 (d, *J* = 7.36 Hz, 1H); b) 7.41 (d, *J* = 7.42 Hz, 1H); c) 7.13 (t, *J* = 7.46 Hz, 1 H); d) 7.05 (t, *J* = 7.36 Hz, 1 H); e) 6.55 (s, 4H); f) 2.09 (s, 6H); g) 1.50 (s, 6H); h) 1.10 (s, 6H),
Water, δ: 2.1 (s, 2H),
H_2, δ: 4.57 (s, 2H),
MesCAT-H_2, δ: i) 8.62 (dd, ^{HH}J = 3.92 Hz, ^{HN}J = 71.56 Hz, 1H) ppm.

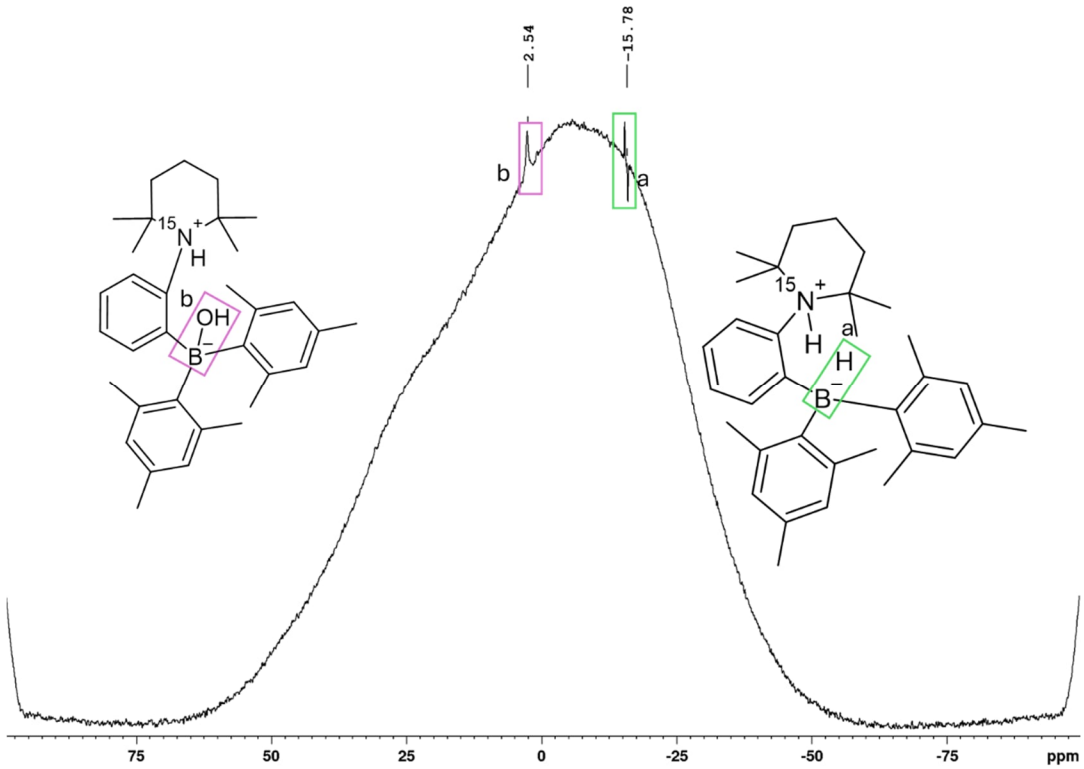

Figure S18. ^{11}B NMR spectrum of a 1 mM solution of MesCAT-H_2O, parahydrogen (6 bars), and 100 equivalents of H_2O in acetonitrile-d3 at 308 K with assignments of the signals. The antiphase signal marked with a green rectangle corresponds to the hyperpolarized **MesCAT-H_2** which was generated in the solution.

Number of accumulations (NS parameter): 256
^{11}B NMR (128.38 MHz, acetonitrile-d3):
MesCAT-H_2, δ: a) -15.78 (d, ^{BH}J = 71.5 Hz, 1B),
MesCAT-H_2O, δ: b) 2.54 (s, 1B) ppm.

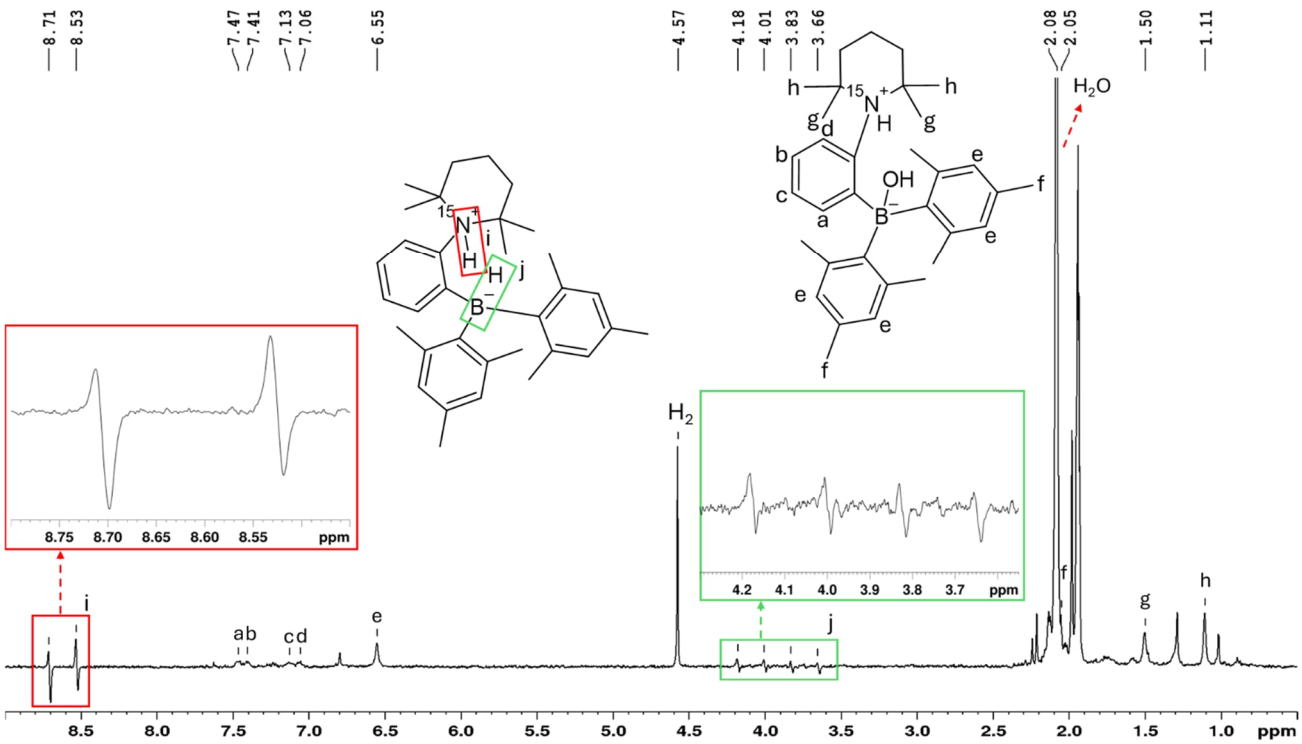

Figure S19. ^{1}H NMR spectrum of a 1 mM solution of MesCAT-H_2O, parahydrogen (6 bars), and 100 equivalents of H_2O in acetonitrile-d3 at 318 K with assignments of the signals. The insets show the antiphase signals corresponding to the ^{15}N-H group (red, two antiphase doublets) and the ^{11}B-H group (green, four antiphase doublets) protons of the hyperpolarized **MesCAT-H_2**, which was generated in the solution.

Number of accumulations (NS parameter): 1
^{1}H NMR (400.13 MHz, acetonitrile-d3):
MesCAT-H_2O, δ: a) 7.47 (d, *J* = 7.12 Hz, 1H); b) 7.41 (d, *J* = 6.24 Hz, 1H); c) 7.13 (t, *J* = 6.40 Hz, 1H); d) 7.06 (t, *J* = 6.45, 1H); e) 6.55 (s, 4H); f) 2.05 (s, 6H); g) 1.50 (s, 6H); h) 1.10 (s, 6H),
Water, δ: 2.08 (s, 2H),
H_2, δ: 4.54 (s, 2H),
MesCAT-H_2, δ: i) 8.62 (dd, ^{HH}J = 3.92 Hz, ^{HN}J = 71.56 Hz, 1H); j) 3.92 (quartet of doublets, ^{HH}J = 3.92 Hz, ^{HB}J = 71.5, 1H) ppm.

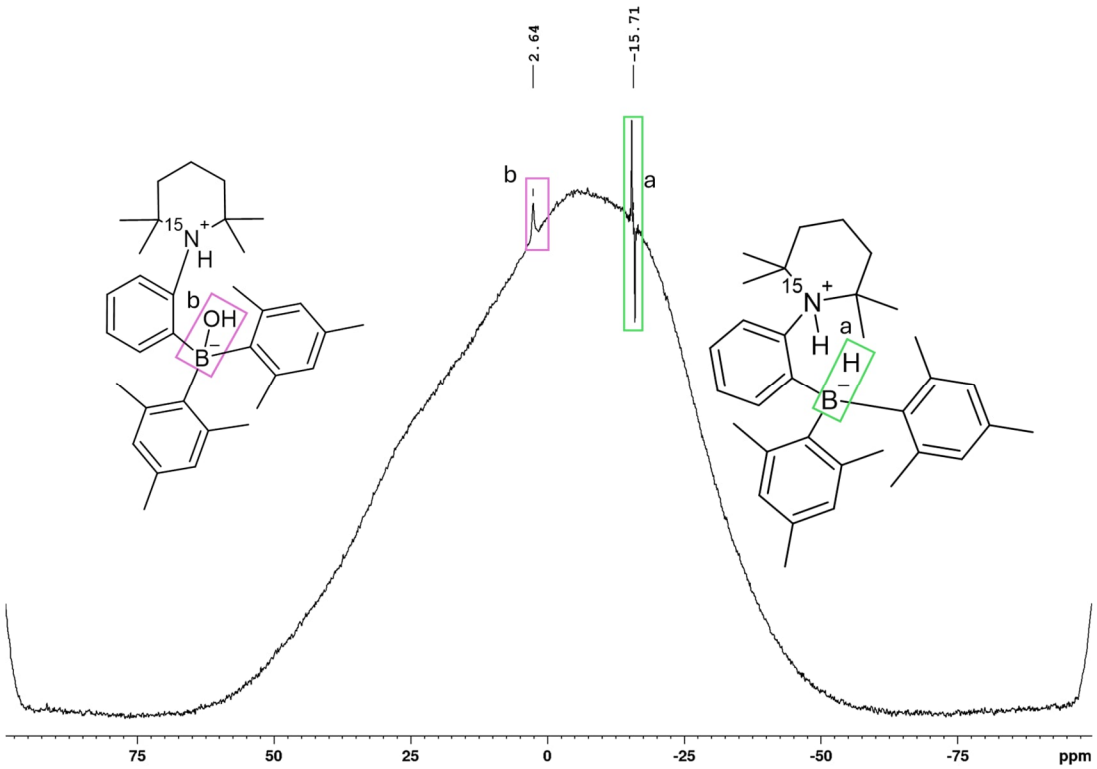

Figure S20. ^{11}B NMR spectrum of a 1 mM solution of MesCAT-H_2O, parahydrogen (6 bars), and 100 equivalents of H_2O in acetonitrile-d3 at 318 K with assignments of the signals. The antiphase signal marked with a green rectangle corresponds to the hyperpolarized **MesCAT-H_2** which was generated in the solution.

Number of accumulations (NS parameter): 256
^{11}B NMR (128.38 MHz, acetonitrile-d3):
MesCAT-H_2, δ: a) -15.71 (d, ^{BH}J = 71.5 Hz, 1B),
MesCAT-H_2O, δ: b) 2.64 (s, 1B) ppm.

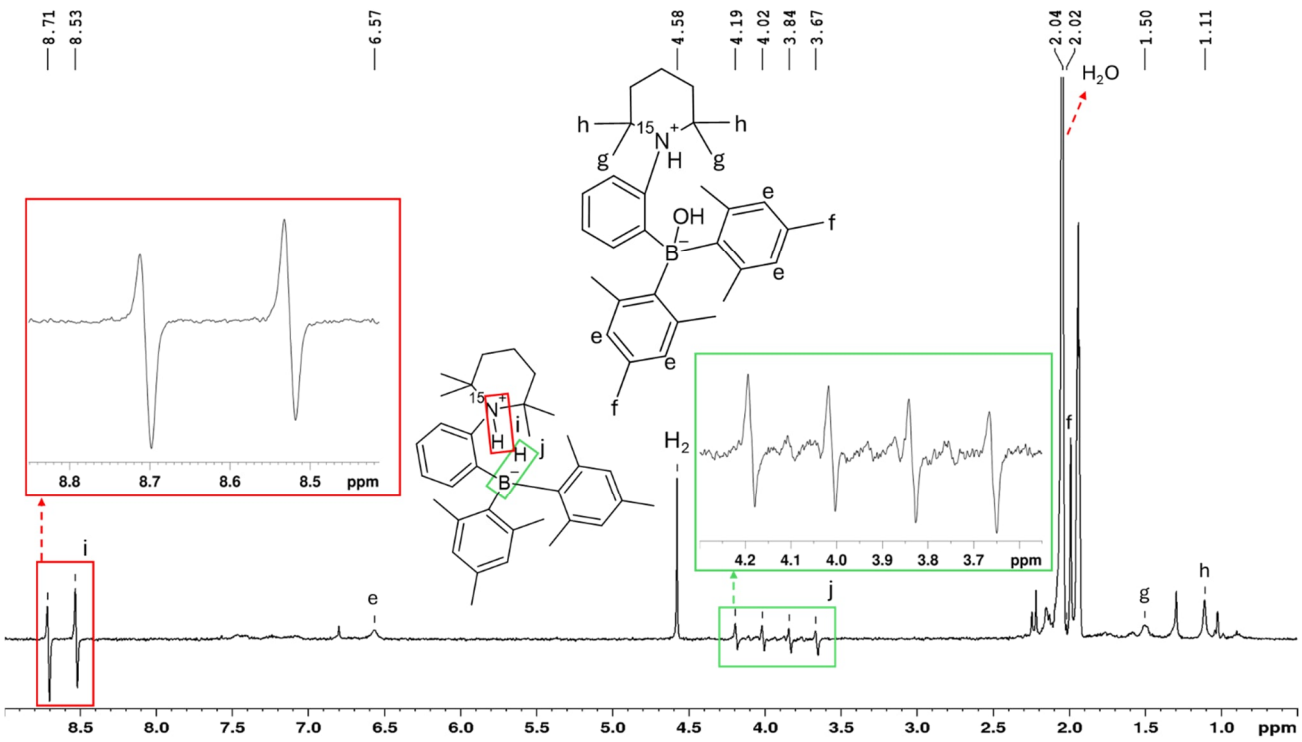

Figure S21. ^{1}H NMR spectrum of a 1 mM solution of MesCAT-H_2O, parahydrogen (6 bars), and 100 equivalents of H_2O in acetonitrile-d3 at 328 K with assignments of the signals. The insets show the antiphase signals corresponding to the ^{15}N-H group (red, two antiphase doublets) and the ^{11}B-H group (green, four antiphase doublets) protons of the hyperpolarized **MesCAT-H_2**, which was generated in the solution.

Number of accumulations (NS parameter): 1
^{1}H NMR (400.13 MHz, acetonitrile-d3):
MesCAT-H_2O, δ: e) 6.57 (s, 4H); f) 2.02 (s, 6H); g) 1.50 (s, 6H); h) 1.11 (s, 6H),
Water, δ: 2.06 (s, 2H),
H_2, δ: 4.58 (s, 2H),
MesCAT-H_2, δ: i) 8.62 (dd, ^{HH}J = 3.92 Hz, ^{HN}J = 71.56 Hz, 1H); j) 3.92 (quartet of doublets, ^{HH}J = 3.92 Hz, ^{HB}J = 71.5, 1H) ppm.

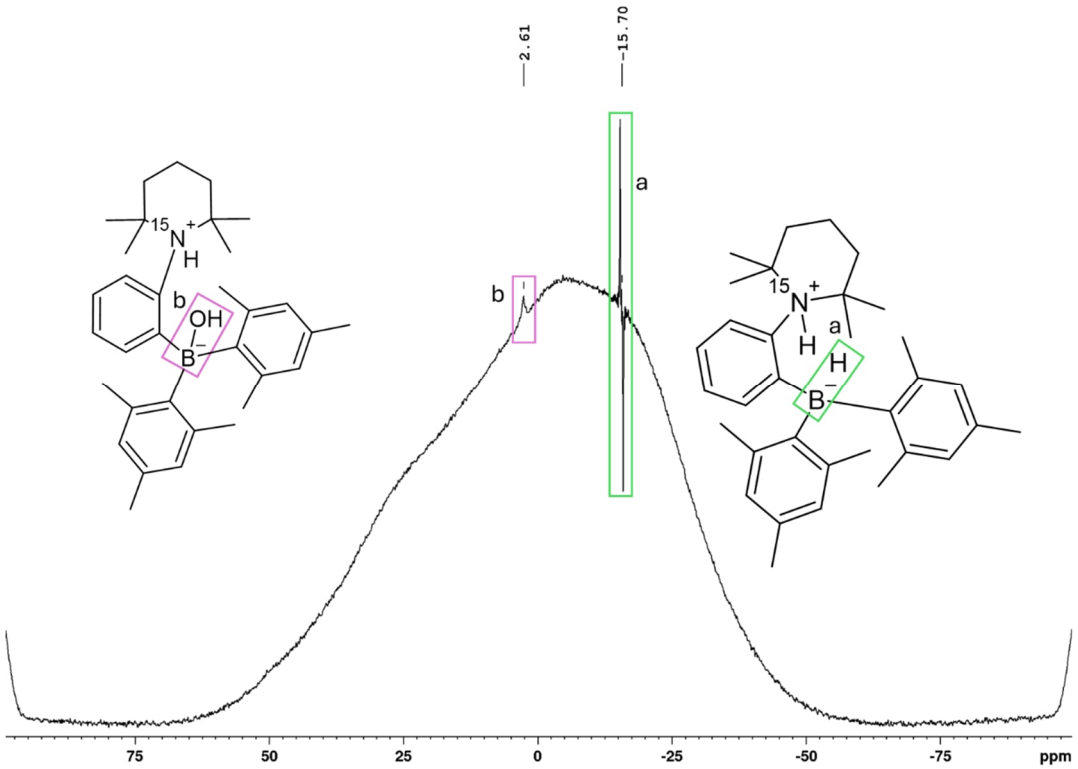

Figure S22. ^{11}B NMR spectrum of a 1 mM solution of MesCAT-H_2O, parahydrogen (6 bars), and 100 equivalents of H_2O in acetonitrile-d3 at 328 K with assignments of the signals. The antiphase signal marked with a green rectangle corresponds to the hyperpolarized **MesCAT-H_2** which was generated in the solution.

Number of accumulations (NS parameter): 256
^{11}B NMR (128.38 MHz, acetonitrile-d3):
MesCAT-H_2, δ: a) 15.70 (d, ^{BH}J = 71.5 Hz, 1B),
MesCAT-H_2O, δ: b) 2.61 (s, 1B) ppm.

3.2 NMR spectra from the experiments with parahydrogen and PhCAT-H_2O

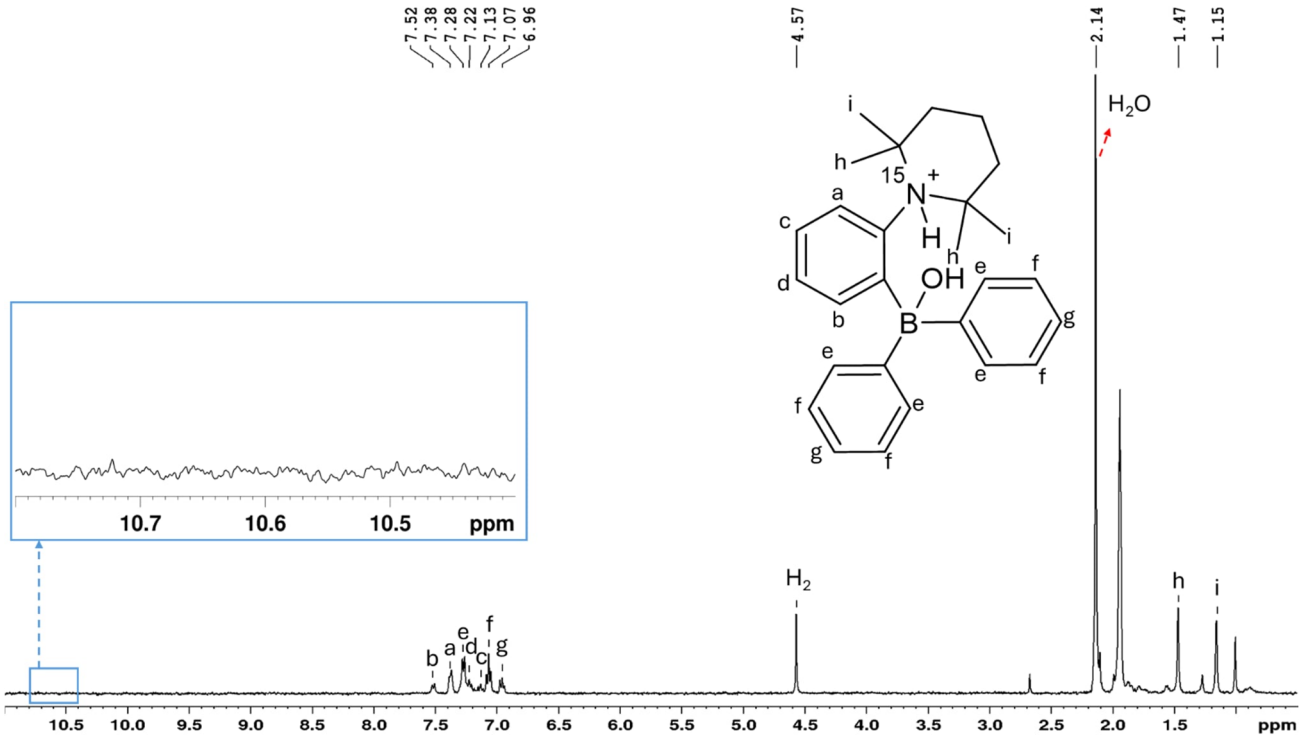

Figure S23. ^{1}H NMR spectrum of a 1 mM solution of PhCAT-H_2O, parahydrogen (6 bars), and 30 equivalents of H_2O in acetonitrile-d3 at 297 K with assignments of the signals. No hyperpolarization effects were observed. The inset shows the aromatic part of the spectrum.

Number of accumulations (NS parameter): 1
^{1}H NMR (400.13 MHz, acetonitrile-d3):
PhCAT-H_2O, δ: b) 7.52 (d, *J* = 4 Hz, 1H); a) 7.38 (d, *J* = 4 Hz, 1H); e) 7.28 (d, *J* = 8 Hz, 4H); d) 7.22 (t, *J* = 6 Hz, 1H); c) 7.13 (t, *J* = 8 Hz, 1H); f) 7.07 (t, *J* = 6 Hz, 4H); g) 6.96 (t, *J* = 8 Hz, 2H); h) 1.47 (s, 4H); i) 1.15 (s, 4H),
Water, δ: 2.14 (s, 2H),
H_2, δ: 4.57 (s, 2H) ppm.

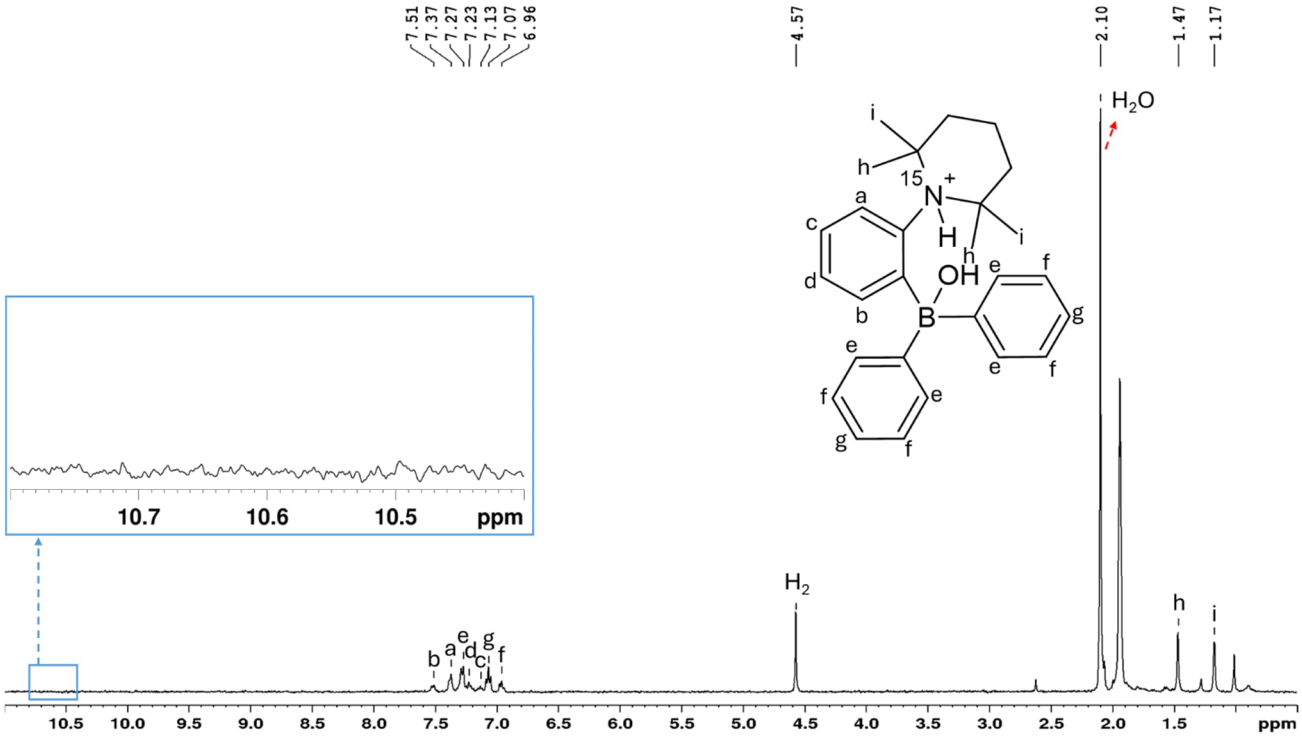

Figure S24. [1]H NMR spectrum of a 1 mM solution of PhCAT-H_2O, parahydrogen (6 bars), and 30 equivalents of H_2O in acetonitrile-d3 at 308 K with assignments of the signals. No hyperpolarization effects were observed. The inset shows the aromatic part of the spectrum.

Number of accumulations (NS parameter): 1
^{1}H NMR (400.13 MHz, acetonitrile-d3):
PhCAT-H_2O, δ: b) 7.51 (d, *J* = 8 Hz, 1H); a) 7.37 (d, *J* = 8 Hz, 1H); e) 7.27 (d, *J* = 8 Hz, 4H); d) 7.23 (t, *J* = 8Hz, 1H); c) 7.13 (t, *J* = 8 Hz, 1H); f) 7.07 (t, *J* = 8 Hz, 4H); g) 6.96 (t, *J* = 8 Hz, 2H); h) 1.47 (s, 4H); i) 1.17 (s, 4H),
Water, δ: 2.10 (s, 2H),
H_2, δ: 4.57, (s, 2H) ppm.

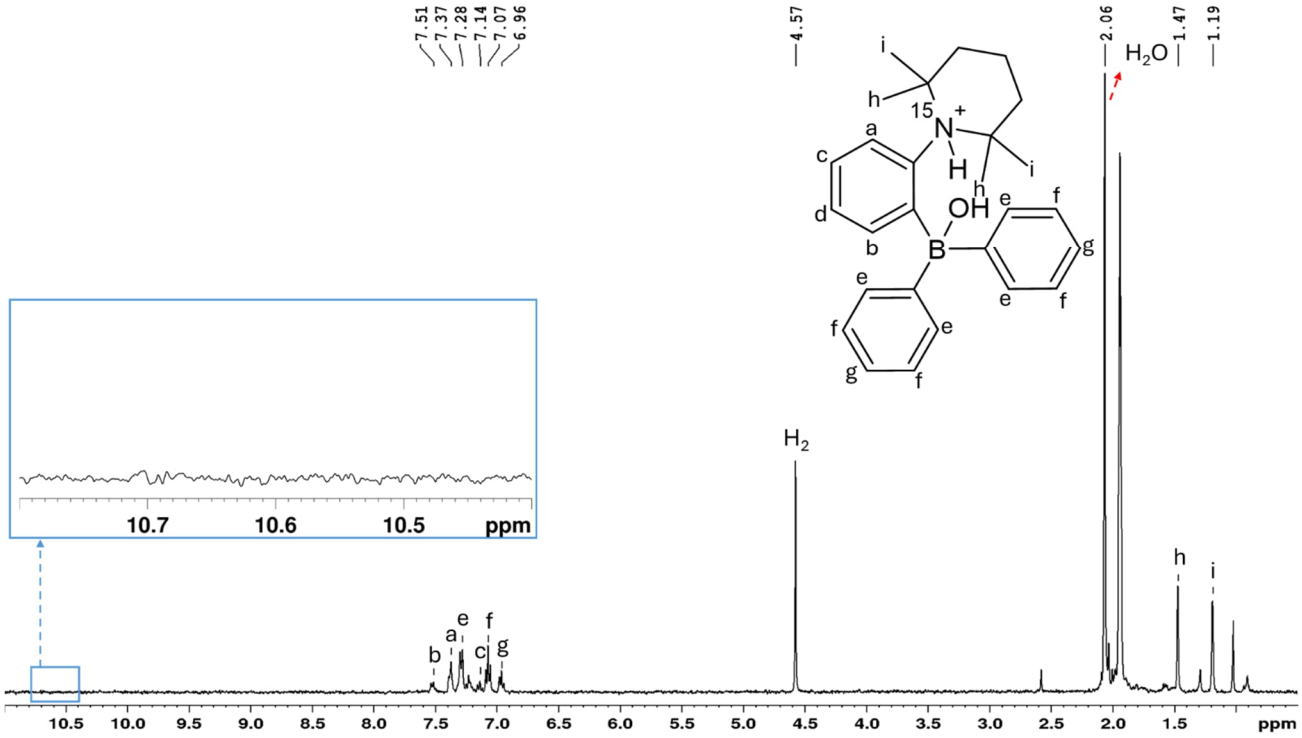

Figure S25. ^{1}H NMR spectrum of a 1 mM solution of PhCAT-H_2O, parahydrogen (6 bars), and 30 equivalents of H_2O in acetonitrile-d3 at 318 K with assignments of the signals. No hyperpolarization effects were observed. The inset shows the aromatic part of the spectrum.

Number of accumulations (NS parameter): 1
^{1}H NMR (400.13 MHz, acetonitrile-d3):
PhCAT-H_2O, δ: b) 7.51 (d, *J* = 8 Hz, 1H); a) 7.37 (d, *J* = 8 Hz, 1H); e) 7.28 (d, *J* = 8 Hz, 4H); c) 7.14 (t, *J* = 6 Hz, 1H); f) 7.07 (t, *J* = 8 Hz, 4H); g) 6.96 (t, *J* = 8 Hz, 2H); h) 1.47 (s, 4H); i) 1.19 (s, 4H),
Water, δ: 2.06 (s, 2H),
H_2, δ: 4.57 (s, 2H) ppm.

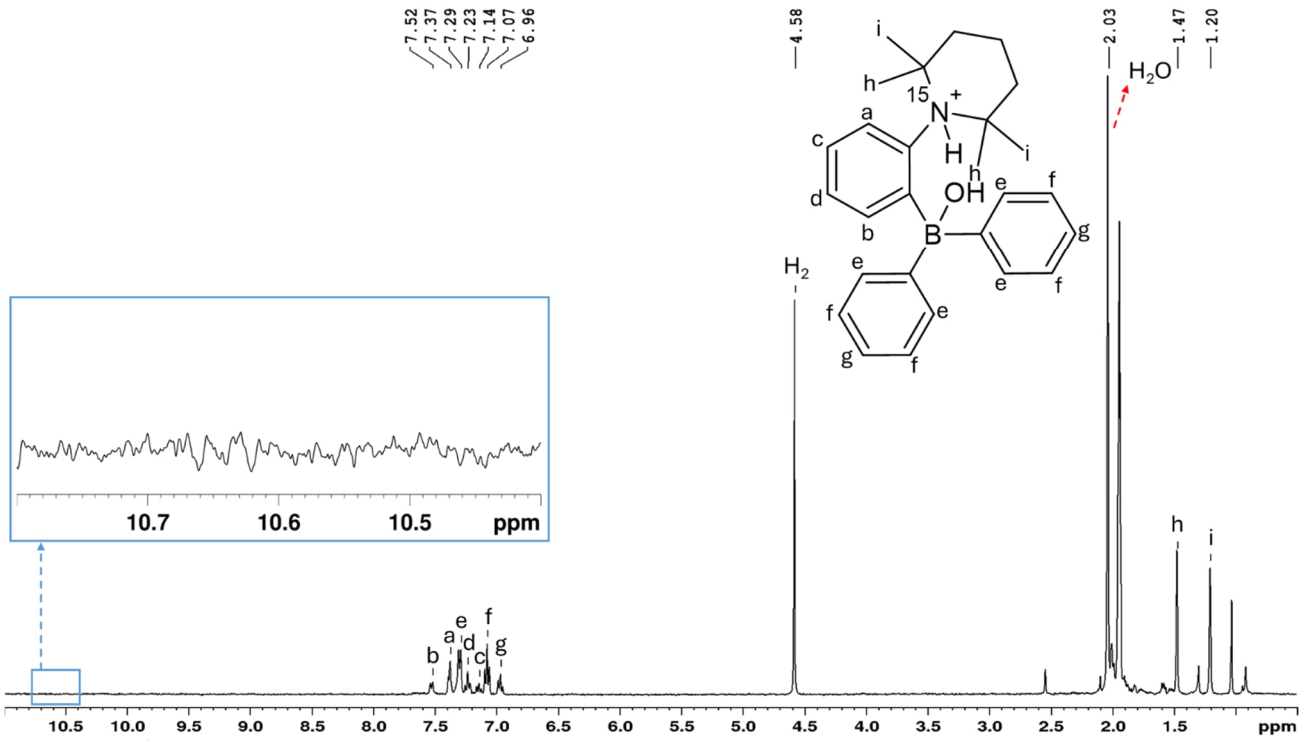

Figure S26. ^{1}H NMR spectrum of a 1 mM solution of PhCAT-H_2O, parahydrogen (6 bars), and 30 equivalents of H_2O in acetonitrile-d3 at 328 K with assignments of the signals. No hyperpolarization effects were observed. The inset shows the aromatic part of the spectrum.

Number of accumulations (NS parameter): 1
^{1}H NMR (400.13 MHz, acetonitrile-d3):
PhCAT-H_2O, δ: b) 7.52 (d, *J* = 8 Hz, 1H); a) 7.37 (d, *J* = 8 Hz, 1H); e) 7.29 (d, *J* = 8 Hz, 4H); d) 7.23 (t, *J* = 8Hz, 1H); c) 7.14 (t, *J* = 8 Hz, 1H); f) 7.07 (t, *J* = 6 Hz, 4H); g) 6.96 (t, *J* = 6 Hz, 2H); h) 1.47 (s, 4H); i) 1.20 (s, 4H),
Water, δ: 2.03 (s, 2H),
H_2, δ: 4.58 (s, 2H) ppm.

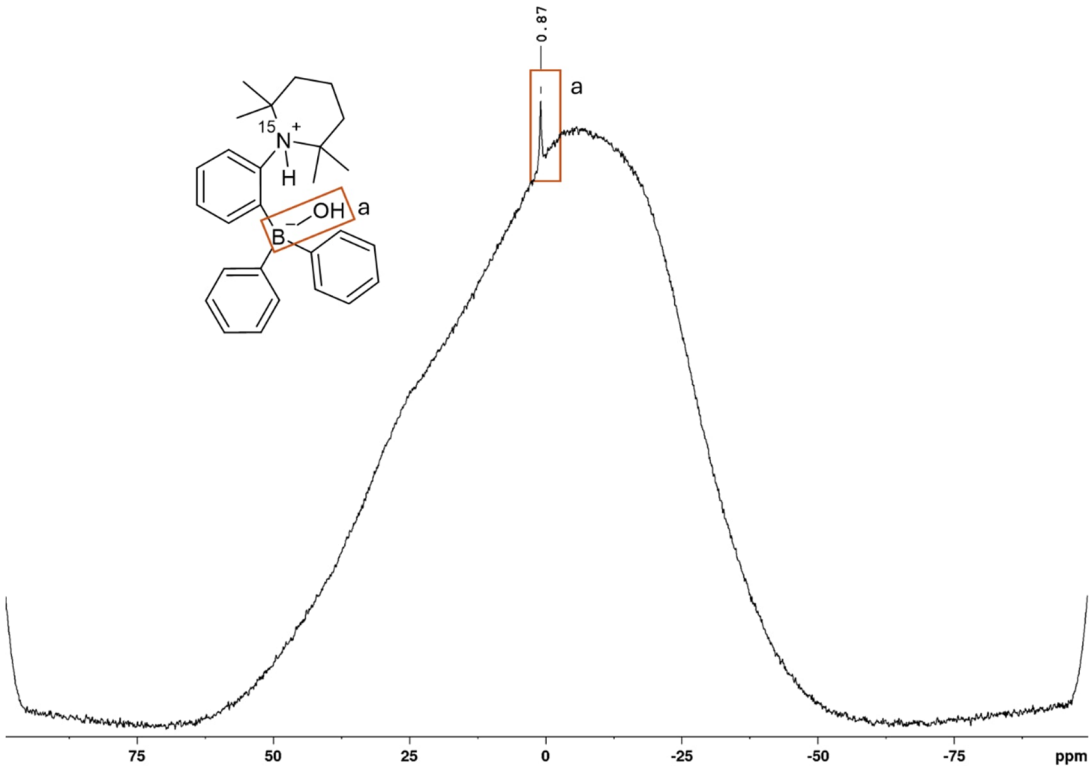

Figure S27. ^{11}B NMR spectrum of a 1 mM solution of **PhCAT-H$_2$O**, parahydrogen (6 bars), and 30 equivalents of H_2O in acetonitrile-d3 at 328 K with assignments of the signals. No hyperpolarization effects were observed. The inset shows the **PhCAT-H$_2$O** signal. The **PhCAT-H$_2$** was not detected.

Number of accumulations (NS parameter): 256
^{11}B NMR (128.38 MHz, acetonitrile-d3):
PhCAT-H$_2$O, δ: a) 0.87 (s, 1B) ppm.

3.3 NMR spectra of MesCAT-H_2O after the relaxation

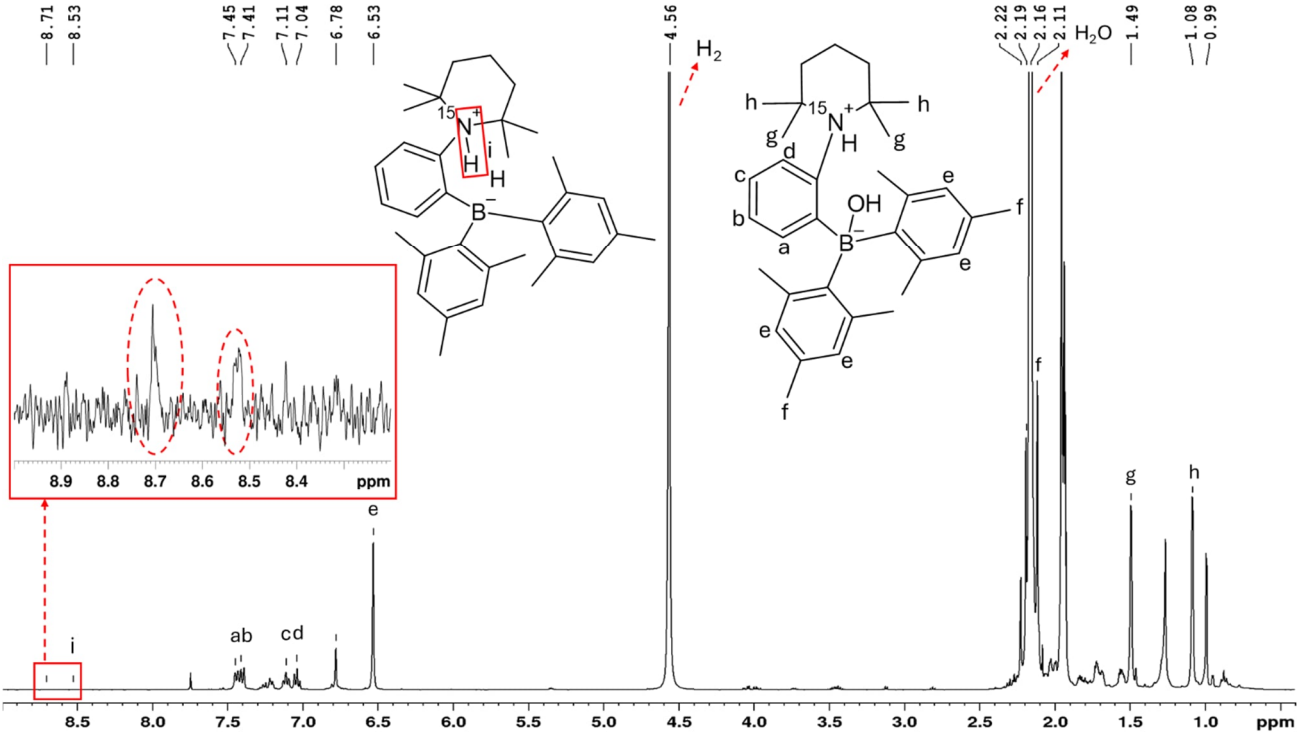

Figure S28. ^{1}H NMR spectrum of a 1 mM solution of MesCAT-H_2O, relaxed parahydrogen (6 bars), and 100 equivalents of H_2O in acetonitrile-d3 at 297 K with assignments of the signals. The inset shows the thermal signals corresponding to ^{15}N-H proton of **MesCAT-H_2** after the relaxation.

Number of accumulations (NS parameter): 3072
^{1}H NMR (400.13 MHz, acetonitrile-d3):
MesCAT-H_2O, δ: a) 7.46 (d, *J* = 8 Hz, 1H); b) 7.42 (d, *J* = 8 Hz, 1H); c) 7.12 (t, *J* = 7.38 Hz, 1H); d) 7.04 (t, *J* = 7.36 Hz, 1H); e) 6.55 (s, 4H); f) 2.12 (s, 6H); g) 1.50 (s, 6H); h) 1.09 (s, 6H),
Water, δ: 2.16 (s, 2H),
H_2, δ: 4.57 (s, 2H),
MesCAT-H_2, δ: i) 8.62 (dd, ^{HN}J = 71.56 Hz, the smaller constant is not resolved) ppm.

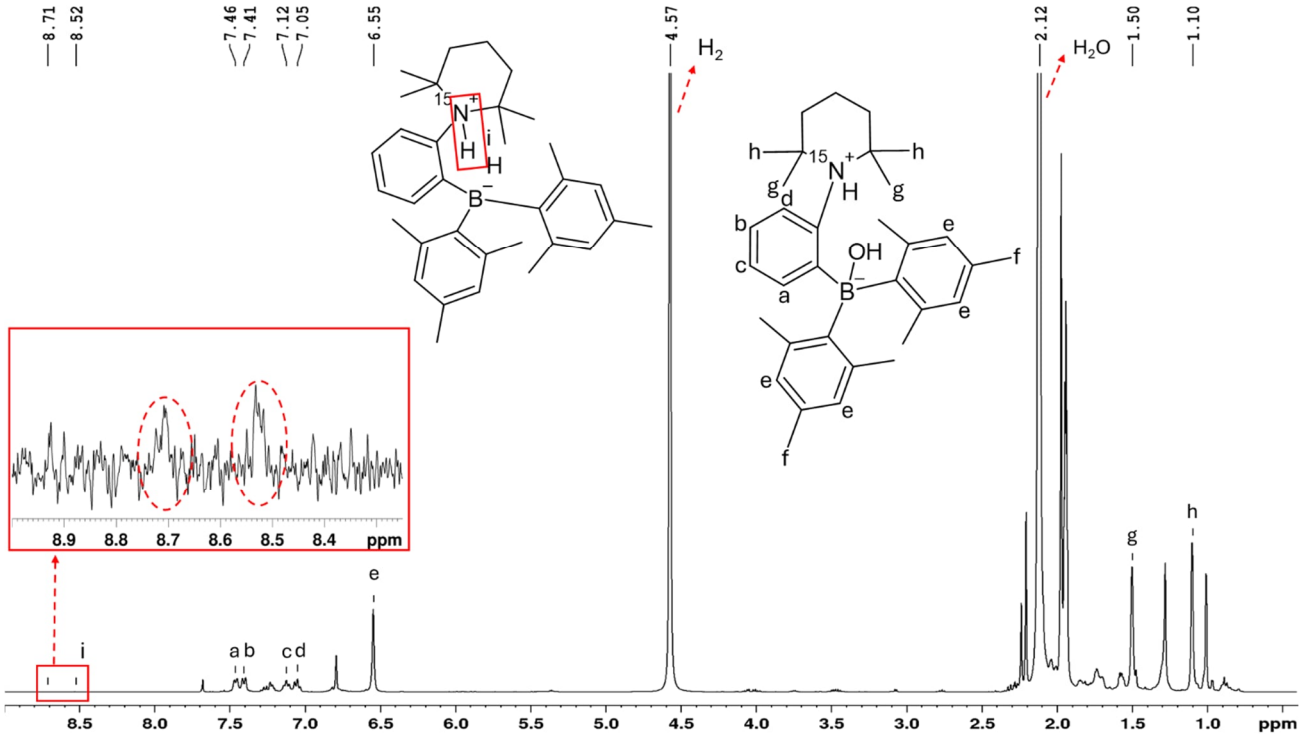

Figure S29. ^{1}H NMR spectrum of a 1 mM solution of MesCAT-H_2O, relaxed parahydrogen (6 bars), and 100 equivalents of H_2O in acetonitrile-d3 at 308 K with assignments of the signals. The inset shows the thermal signals corresponding to the ^{15}N-H proton of **MesCAT-H_2** after the relaxation.

Number of accumulations (NS parameter): 3072
^{1}H NMR (400.13 MHz, acetonitrile-d3):
MesCAT-H_2O, δ: a) 7.45 (d, *J* = 7.32 Hz, 1H); b) 7.39 (d, *J* = 7.52 Hz, 1H); c) 7.12 (t, *J* = 7.20 Hz, 1H); d) 7.05 (t, *J* = 7.20 Hz, 1H); e) 6.54 (s, 4 H); f) 2.09 (s, 6H); g) 1.50 (s, 6H); h) 1.10 (s, 6H),
Water, δ: 2.12 (s, 2H),
H_2, δ: 4.57 (s, 2H),
MesCAT-H_2, δ: i) 8.62 (dd, ^{HN}J = 71.56 Hz, the smaller constant is not resolved) ppm.

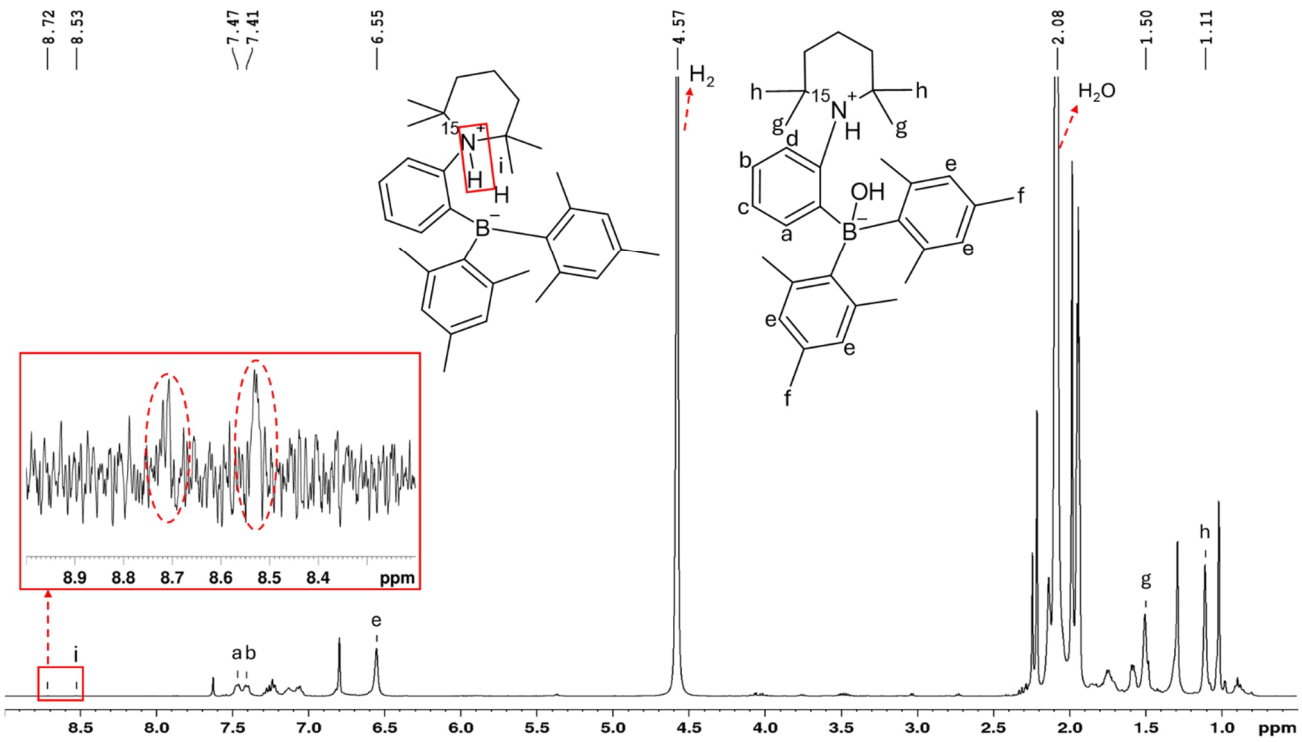

Figure S30. ^{1}H NMR spectrum of a 1 mM solution of MesCAT-H_2O, relaxed parahydrogen (6 bars), and 100 equivalents of H_2O in acetonitrile-d3 at 318 K with assignments of the signals. The inset shows the thermal signals corresponding to the ^{15}N-H proton of **MesCAT-H_2** after the relaxation.

Number of accumulations (NS parameter): 3072
^{1}H NMR (400.13 MHz, acetonitrile-d3):
MesCAT-H_2O, δ: a) 7.46 (d, *J* = 6.68 Hz, 1H); b) 7.41 (d, *J* = 6.68 Hz, 1H); e) 6.55 (s, 4H); g) 1.50 (s, 6H); h) 1.11 (s, 6H),
Water, δ: 2.08 (s, 2H),
H_2, δ: 4.57 (s, 2H),
MesCAT-H_2, δ: i) 8.62 (dd, ^{HN}J = 71.56 Hz, the smaller constant is not resolved) ppm.

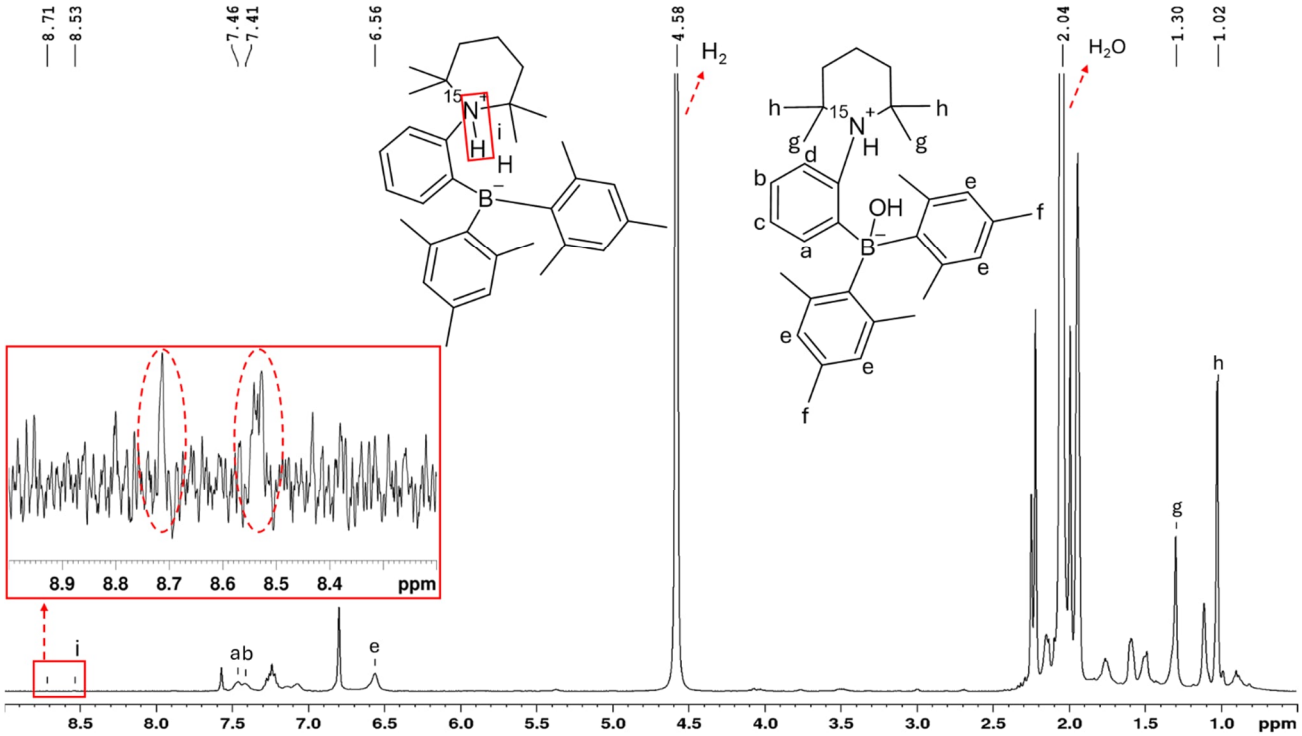

Figure S31. ^{1}H NMR spectrum of a 1 mM solution of MesCAT-H_2O, relaxed parahydrogen (6 bars), and 100 equivalents of H_2O in acetonitrile-d3 at 328 K with assignments of the signals. The inset shows the thermal signals corresponding to the ^{15}N-H proton of **MesCAT-H_2** after the relaxation.

Number of accumulations (NS parameter): 3072
^{1}H NMR (400.13 MHz, acetonitrile-d3):
MesCAT-H_2O, δ: a) 7.47 (s, 1H); b) 7.43 (d, 1H); e) 6.56 (s, 4H); g) 1.29 (s, 6H); h) 1.02 (s, 6H),
Water, δ: 2.04 (s, 2H),
H_2, δ: 4.58 (s, 2H),
MesCAT-H_2, δ: i) 8.62 (dd, ^{HN}J = 71.56 Hz, the smaller constant is not resolved) ppm.

3.4 NMR spectra of PhCAT-H₂O after the relaxation

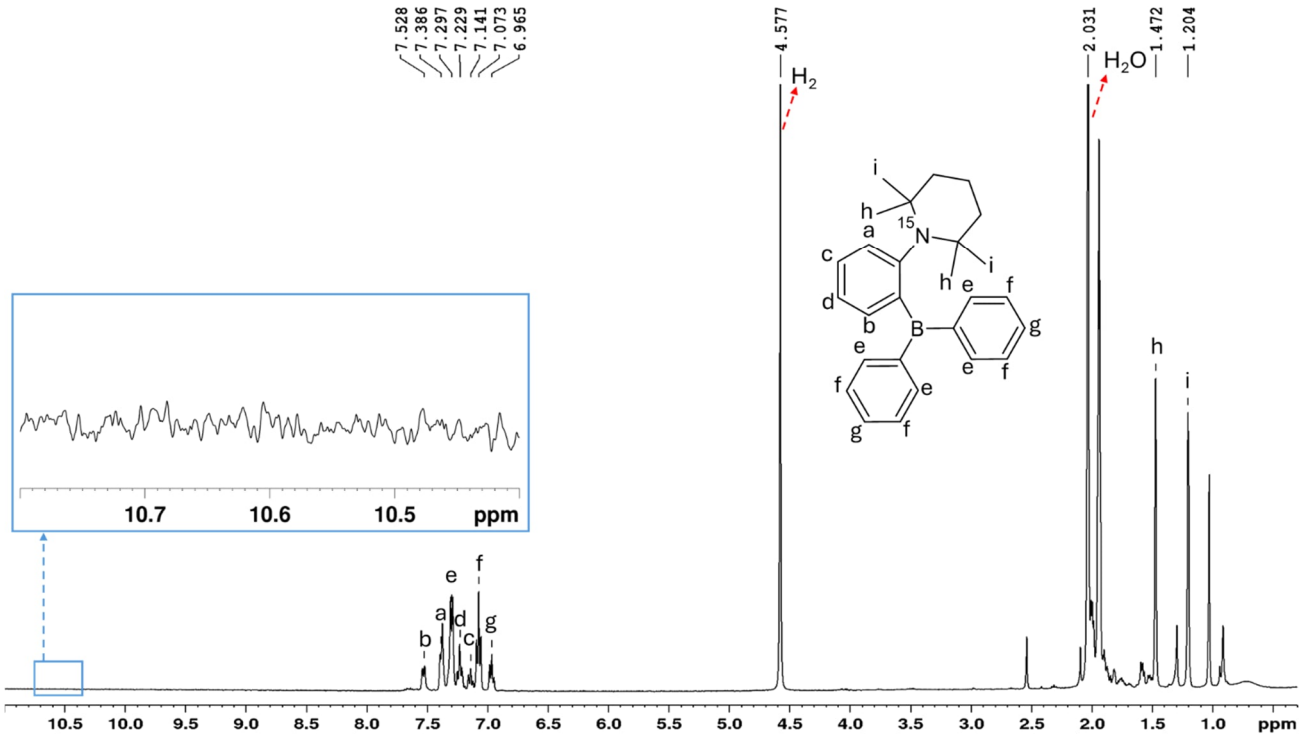

Figure S32. ^{1}H NMR spectrum of a 1 mM solution of PhCAT-H_2O, relaxed parahydrogen (6 bars), and 20 equivalents of H_2O in acetonitrile-d3 at 328 K with assignments of the signals. The inset shows the region in which the thermal signals corresponding to the ^{15}N-H proton of **PhCAT-H₂** should appear after the relaxation if these species were to form in the solution.

Number of accumulations (NS parameter): 256
^{1}H NMR (400.13 MHz, acetonitrile-d3):
PhCAT, δ: b) 7.53 (d, *J* = 7.20 Hz, 1H); a) 7.39 (d, *J* = 7.20 Hz, 1H); e) 7.30 (d, *J* = 7.20 Hz, 4H); d) 7.23 (t, *J* = 7.26 Hz, 1H); c) 7.14 (t, *J* = 7.20 Hz, 1H); f) 7.07 (t, *J* = 7.20 Hz, 4H); g) 6.96 (t, *J* = 7.20 Hz, 2H); h) 1.47 (s, 4H); i) 1.20 (s, 4H),
Water, δ: 2.03 (s, 2H),
H₂, δ: 4.58 (s, 2H) ppm.

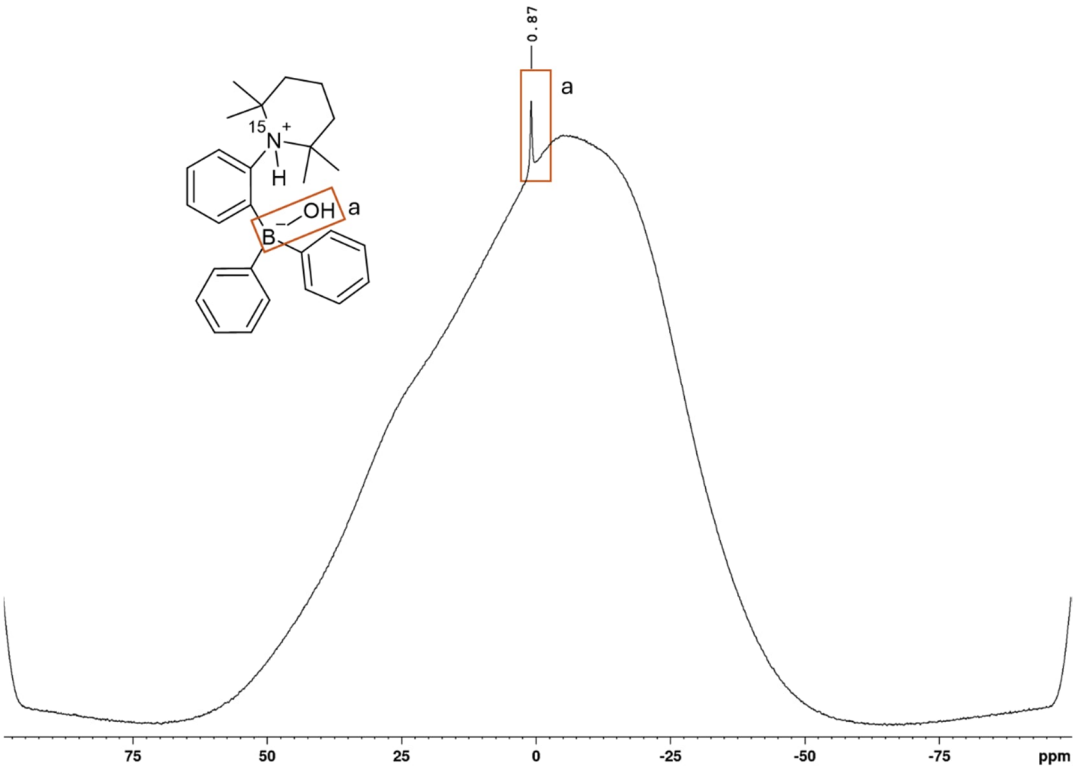

Figure S33. ^{11}B NMR spectrum of a 1 mM solution of **PhCAT-H$_2$O**, relaxed parahydrogen (6 bars), and 30 equivalents of H_2O in acetonitrile-d3 at 328 K with assignments of the signals. The inset shows the **PhCAT-H$_2$O** signal. The **PhCAT-H$_2$** was not detected.

Number of accumulations (NS parameter): 4096
^{11}B NMR (128.38 MHz, acetonitrile-d3):
PhCAT-H$_2$O, δ: a) 0.87 (s, 1H) ppm.

4 References

S1. K. Sorochkina, V. V. Zhivonitko, K. Chernichenko, V. V. Telkki, T. Repo and I. V. Koptyug, *J. Phys. Chem. Lett.*, 2018, **9**, 903-907.

S2. C. R. Bowers, in *Encyclopedia of Nuclear Magnetic Resonance*, eds. D. M. Grant and R. K. Harris, Wiley, Chichester, 2002, vol. 9, ch. Chapter, pp. 750-769.

S3. E. Brunner, *J. Chem. Eng. Data*, 1985, **30**, 269-273.

S4. M. B. Krüger, C. Selle, D. Heller and W. Baumann, *J. Chem. Eng. Data*, 2012, **57**, 1737-1744.

S5. K. Konsewicz, G. Laczkó, I. Pápai and V. V. Zhivonitko, *Phys. Chem. Chem. Phys.*, 2024, **26**, 3197-3207.

S6. J. Jeener, B. H. Meier, P. Bachmann and R. R. Ernst, *J. Chem. Phys.*, 1979, **71**, 4546-4553.

S7. M. J. Frisch, G. W. Trucks, H. B. Schlegel, G. E. Scuseria, M. A. Robb, J. R. Cheeseman, G. Scalmani, V. Barone, G. A. Petersson, H. Nakatsuji, X. Li, M. Caricato, A. V. Marenich, J. Bloino, B. G. Janesko, R. Gomperts, B. Mennucci, H. P. Hratchian, J. V. Ortiz, A. F. Izmaylov, J. L. Sonnenberg, D. Williams-Young, F. Ding, F. Lipparini, F. Egidi, J. Goings, B. Peng, A. Petrone, T. Henderson, D. Ranasinghe, V. G. Zakrzewski, J. Gao, N. Rega, G. Zheng, W. Liang, M. Hada, M. Ehara, K. Toyota, R. Fukuda, J. Hasegawa, M. Ishida, T. Nakajima, Y. Honda, O. Kitao, H. Nakai, T. Vreven, K. Throssell, J. A. Montgomery Jr., J. E. Peralta, F. Ogliaro, M. J. Bearpark, J. J. Heyd, E. N. Brothers, K. N. Kudin, V. N. Staroverov, T. A. Keith, R. Kobayashi, J. Normand, K. Raghavachari, A. P. Rendell, J. C. Burant, S. S. Iyengar, J. Tomasi, M. Cossi, J. M. Millam, M. Klene, C. Adamo, R. Cammi, J. W. Ochterski, R. L. Martin, K. Morokuma, O. Farkas, J. B. Foresman and D. J. Fox, *Gaussian 16 Rev. E.01*, Wallingford CT, 2016.

S8. J. D. Chai and M. Head-Gordon, *Phys. Chem. Chem. Phys.*, 2008, **10**, 6615-6620.

S9. S. Grimme, *Chem. Eur. J.*, 2012, **18**, 9955-9964.

S10. A. V. Marenich, C. J. Cramer and D. G. Truhlar, *J. Phys. Chem. B*, 2009, **113**, 6378-6396.